Article

Cell Host & Microbe

# A nucleoside signal generated by a fungal endophyte regulates host cell death and promotes root colonization

## Graphical abstract

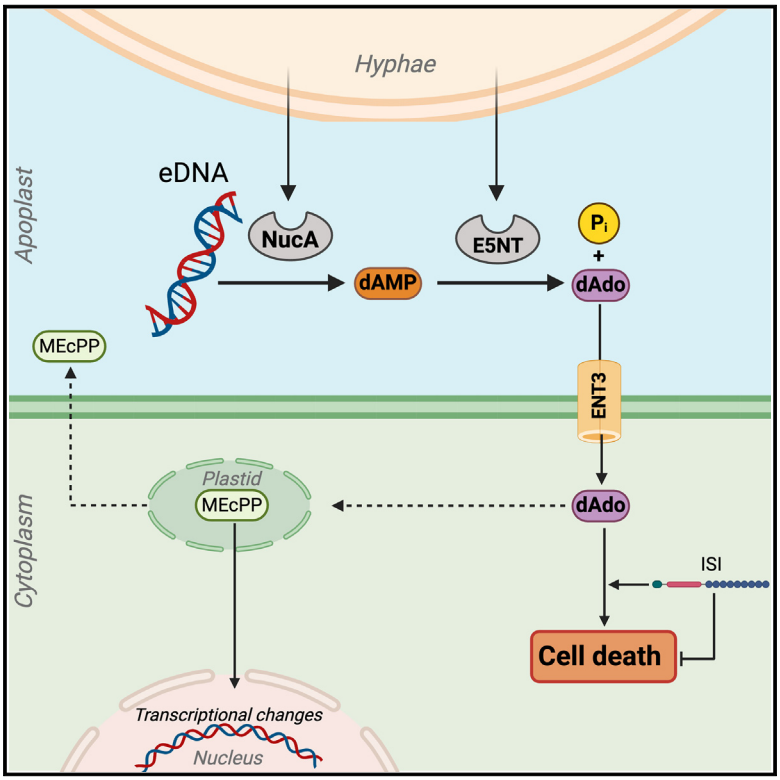


## Authors

Nick Dunken, Heidi Widmer, Gerd U. Balcke, ..., Alain Tissier, Claus-Peter Witte, Alga Zuccaro

## Correspondence

azuccaro@uni-koeln.de

## In brief

Dunken and colleagues find that the beneficial root endophytic fungus *Serendipita indica* secretes two effector enzymes into the host apoplast to produce deoxyadenosine (dAdo). dAdo triggers host cell death and other immune responses in an ENT3-dependent manner. This process is influenced by the TIR-NLR protein *AtISI* and promotes root colonization.

## Highlights

- Two apoplastic enzymes from a beneficial root endophytic fungus synergistically produce dAdo
- dAdo is a potent inducer of plant cell death
- ENT3 transporter is essential for dAdo uptake and modulates fungal-elicited cell death
- Mutations in the *At*ISI locus reduce dAdo-induced cell death and affect fungal colonization

Dunken et al., 2024, Cell Host & Microbe *32*, 2161–2177
December 11, 2024 
https://doi.org/10.1016/j.chom.2024.10.020

CellPress

Cell Host & Microbe

CellPress
OPEN ACCESS

Article

# A nucleoside signal generated by a fungal endophyte regulates host cell death and promotes root colonization

Nick Dunken,[1] Heidi Widmer,[1,5] Gerd U. Balcke,[2] Henryk Straube,[3,4] Gregor Langen,[1] Nyasha M. Charura,[1] Pia Saake,[1,5] Concetta De Quattro,[1,5] Jonas Schön,[5,6] Hanna Rövenich,[1,5] Stephan Wawra,[1,5] Mamoona Khan,[7] Armin Djamei,[7] Matias D. Zurbriggen,[5,6] Alain Tissier,[2,8] Claus-Peter Witte,[3] and Alga Zuccaro[1,5,9,*]

[1]Institute for Plant Sciences, University of Cologne, Cologne, Germany
[2]Department of Cell and Metabolic Biology, Leibniz Institute of Plant Biochemistry, Halle, Germany
[3]Molecular Nutrition and Biochemistry of Plants, Leibniz University Hannover, Herrenhäuser Str. 2, 30419 Hannover Germany
[4]Section for Plant Biochemistry and Copenhagen Plant Science Centre, Department of Plant and Environmental Sciences, University of Copenhagen, Frederiksberg, Denmark
[5]Cluster of Excellence on Plant Sciences (CEPLAS), Cologne, Germany
[6]Institute of Synthetic Biology, Heinrich-Heine-Universität Düsseldorf, Düsseldorf, Germany
[7]Department of Plant Pathology, Institute of Crop Science and Resource Conservation (INRES), University of Bonn, Bonn, Germany
[8]Institute of Pharmacy, Martin-Luther University Halle-Wittenberg, Halle, Germany
[9]Lead contact
*Correspondence: azuccaro@uni-koeln.de
https://doi.org/10.1016/j.chom.2024.10.020

## SUMMARY

The intracellular colonization of plant roots by the beneficial fungal endophyte *Serendipita indica* follows a biphasic strategy, including a host cell death phase that enables successful colonization of *Arabidopsis thaliana* roots. How host cell death is initiated and controlled is largely unknown. Here, we show that two fungal enzymes, the ecto-5′-nucleotidase *Si*E5NT and the nuclease *Si*NucA, act synergistically in the apoplast at the onset of cell death to produce deoxyadenosine (dAdo). The uptake of extracellular dAdo but not the structurally related adenosine activates cell death via the equilibrative nucleoside transporter ENT3. We identified a previously uncharacterized Toll-like interleukin 1 receptor (TIR)-nucleotide-binding leucine-rich repeat receptor (NLR) protein, ISI (induced by *S. indica*), as an intracellular factor that affects host cell death, fungal colonization, and growth promotion. Our data show that the combined activity of two fungal apoplastic enzymes promotes the production of a metabolite that engages TIR-NLR-modulated pathways to induce plant cell death, providing a link to immunometabolism in plants.

## INTRODUCTION

Regulated cell death (RCD) occurs in plants as part of normal growth and development and in response to abiotic and biotic stimuli. In plant-microbe interactions, host cell death programs can mediate either resistance or successful infection. Depending on the type of microbial lifestyle, host cell death can benefit the plant by stopping the growth of biotrophs or the microbe by promoting the growth of necrotrophs. Thus, control of plant host cell death is critical to the outcome of an interaction. Host cell death also plays a role in certain beneficial interactions, challenging the paradigm that cell death in plant-microbe interactions implies pathogenesis or host-microbe incompatibility. Both symbiosis with beneficial microbes and infection by pathogens require sophisticated control of host defenses and nutrient fluxes. Certain features of the interaction of beneficial microbes, such as affecting host immunity, metabolism, and host cell death, are reminiscent of pathogen infections. In Rhizobium-legume symbioses, root nodules are formed to provide a niche for bacterial nitrogen fixation. The formation of infection pockets is associated with host cell death and the production of hydrogen peroxide.[1] Host cell death is also observed in ectomycorrhizal symbioses[2,3] and is a requisite for the establishment of symbiotic interactions with the widely distributed beneficial fungi of the order Sebacinales.[4–6] Molecular environmental studies have shown that some of the most abundant taxa of this order have little, if any, host specificity and interact with a wide variety of plant species. Sebacinales isolates, including *S. indica* and *S. vermifera*, exhibit beneficial effects such as growth promotion, increased seed production, and protection from pathogens and thus play an important role in natural and managed ecosystems.[7–9] The requirement of restricted host cell death for the establishment of certain beneficial microorganisms leads to the hypothesis that the activation of cell death mechanisms in roots has a more important ecological function than previously thought.

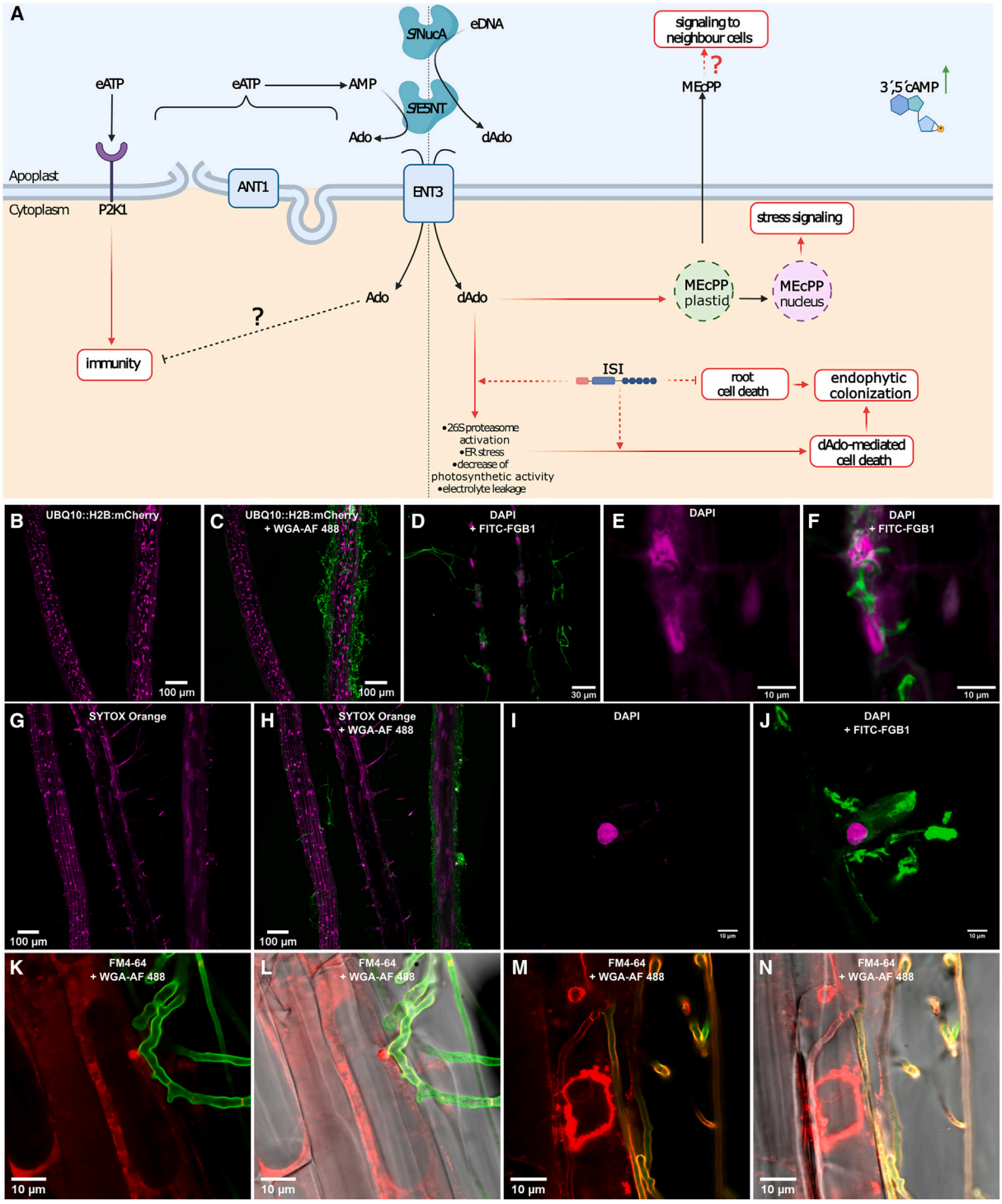


**Figure 1. Host cell death during *S. indica* colonization of roots**

(A) Current model for dAdo-triggered cell death during colonization of *A. thaliana* roots by *S. indica*. The beneficial endophyte *S. indica* secretes two enzymes into the apoplast, the nuclease *Si*NucA and the ecto-nucleotidase *Si*E5NT. *Si*E5NT is initially involved in manipulating eATP signaling (left), as described in Nizam et al.[13] *Si*NucA accumulates at the onset of cell death. The combined activity of *Si*NucA and *Si*E5NT releases deoxynucleosides from DNA, with a strong preference for dAdo, a potent cell death inducer in animal systems. dAdo is transported to the cytoplasm *via* *At*ENT3, where it triggers a cell death process and contributes to successful fungal colonization. dAdo induces the production of the retrograde stress signal MEcPP from plastids, activating stress signaling and possibly intercellular communication. Cell death triggered by dAdo is modulated by an uncharacterized TIR-type NLR protein (ISI, induced by *S. indica*), providing a link to immunometabolism.

*(legend continued on next page)*

In the hosts *Hordeum vulgare* (hereafter barley) and *A. thaliana* (hereafter Arabidopsis), Sebacinales fungi initially colonize living cells that die during the progression of colonization.[4–6,10–12] This symbiotic cell death is thought to contribute to niche differentiation during microbial competition for space and nutrients in the root and appears to be restricted to colonized cells in the epidermis and outer cortex. The host pathways that control the induction and execution of plant cell death and the fungal elicitors/effectors that initiate this process in roots are still largely unknown.[5,6,13,14] Pathogenic and beneficial fungi have a large repertoire of secreted effectors that can affect host cell physiology and suppress plant defenses, promoting fungal colonization. In fungi, effectors have been described mainly in biotrophic and hemibiotrophic foliar pathogens.[15] By contrast, only a few effectors of root symbiotic fungi have been functionally characterized.[13,16–20] Therefore, the modes of action of effectors of mutualistic fungi remain poorly understood.

Using genomics, transcriptomics, and proteomics, we identified proteins secreted by *S. indica* into the root apoplast.[13] One secreted protein consistently found at various stages of symbiosis is the ecto-5′-nucleotidase *Si*E5NT (PIIN_01005).[13] Expression of *SiE5NT is* induced during colonization of barley and Arabidopsis roots but not in axenic fungal culture.[13] Animal ecto-5'-nucleotidases play a key role in the conversion of AMP to adenosine, counteracting the immunogenic effects of extracellular ATP (eATP) released from host cells.[21] eATP is an important signal in plants that controls development and response to biotic and abiotic stresses. In Arabidopsis, eATP mediates various cellular processes through its binding to the purinergic membrane-associated receptor proteins DORN1/P2K1 and P2K2.[22] In the apoplast, eATP accumulation increases cytoplasmic calcium and triggers a defense response against invading microbes. The perception of extracellular nucleotides, such as eATP, plays an important role in plant-fungal interactions—we previously demonstrated this by showing that the knockout (KO) mutant *dorn1* of Arabidopsis is better colonized by *S. indica*. Partially purified preparations of *Si*E5NT are able to hydrolyze adenylates to adenosine, which alters the eATP content in the apoplast and the plant response to fungal colonization.[13] Secretion of *Si*E5NT in Arabidopsis leads to enhanced colonization by *S. indica*, confirming its role as an apoplastic effector protein. Considering the important role *Si*E5NT plays in fungal accommodation at early symbiotic stages, we proposed that modulation of extracellular nucleotide levels and their perception play a key role in compatibility during early plant-fungal interactions in roots.[13] Secreted *Si*E5NT homologs are also present in fungal pathogens such as *Colletotrichium incanum* and *Fusarium oxysporum* and other Arabidopsis endophytes such as *Colletotrichum tofieldiae*, suggesting that purine-based extracellular biomolecules also play a role in other plant-fungal interactions.

During the colonization of barley and Arabidopsis by *S. indica*, a small fungal endonuclease, which we named *Si*NucA (PIIN_02121), is secreted with *Si*E5NT at the onset of cell death.[13,23] In plants, the mechanisms linking immune recognition of DNA danger signals in the extracellular environment to innate signaling pathways in the cytosol are poorly understood, as is the role of (deoxy)nucleotide metabolism in root colonization and cell death. Here, we show that the synergistic activity of *Si*NucA and *Si*E5NT leads to the production of deoxyadenosine (dAdo) from extracellular DNA (eDNA). dAdo production by fungal extracellular enzymes is similar to the processes involved in dAdo-mediated immune cell death of *Staphylococcus aureus* in animals, which appears to ensure bacterial survival in host tissues.[24,25] Staphylococcal nuclease and adenosine synthase A (AdsA, a homolog of *Si*E5NT) are both required to release dAdo from neutrophil extracellular traps (NETs), which has a potent cytotoxic effect on macrophages and other immune cells.[24]

We demonstrate that dAdo but not the structurally similar Ado activates a previously unidentified cell death mechanism in plants. Expression of either extracellular *Si*NucA or *Si*E5NT *in planta* results in enhanced colonization by *S. indica* and host cell death.[13] We found that a mutation in the equilibrative nucleoside transporter 3 (ENT3) of Arabidopsis leads to a strong and specific resistance phenotype to dAdo-induced cell death. Accordingly, the *ent3* KO line shows less fungal-induced cell death in the root and accumulates less of the extracellular signaling metabolite methylerythritol cyclodiphosphate (MEcPP) in response to fungal colonization or dAdo treatment.

Finally, through a mutant screen of Arabidopsis transfer DNA (T-DNA) insertion lines, we identified a previously uncharacterized locus including several Toll-like interleukin 1 receptor (TIR)-nucleotide-binding leucine-rich repeat receptor (NLR) proteins. Mutation in one of these proteins appears to modulate cell death triggered by dAdo, as well as fungal colonization and growth promotion. While most characterized TIR-NLRs (TNLs) function as sensors of pathogen-secreted effectors, our findings suggest that this TNL may be involved in the regulation of cell death induced by a metabolite produced during symbiosis. We hypothesize that the hydrolysis of extracellular metabolites by the fungal enzymes *Si*NucA and *Si*E5NT provides a link between purine metabolism, immunity, and cell death pathways in roots (Figure 1A).

(B and C) Arabidopsis roots expressing the fluorescent nuclear marker UBQ10::H2B:mCherry (magenta) stained with the fungal cell wall marker wheat germ agglutinin Alexa Fluor 488 conjugate WGA-AF 488 (green) at 10 dpi.
(D) Plant nuclei stained with DAPI (magenta) and fungal cell wall and matrix stained with the β-glucan binding lectin FGB1-fluorescein isothiocyanate (FITC) 488 (green) at 6 dpi. As colonization by *S. indica* progresses, host nuclei often become elongated and fade.
(E and F) Close-up of *S. indica* hyphae embedded in a host nucleus from (D).
(G and H) Staining of nucleic acids of roots colonized with *S. indica* with the dead cell indicator (membrane integrity marker) SYTOX Orange (magenta) and fungal hyphae with WGA-AF 488 (green) at 10 dpi.
(I and J) *S. indica* hyphae fluorescently labeled with the β-glucan-binding lectin FGB1-FITC 488 (green) embedded in a DAPI-stained host nucleus (magenta) at 6 dpi.
(K–N) Progressive vacuolar collapse of colonized root cells. Fungal hyphae are stained with WGA-AF 488 (green), while membranes are stained with FM4-64 (red). (J and K) Initial biotrophic colonization. (M and N) Vacuolar collapse in a dying host cell. CLSM was repeated at least five times with 3 to 4 plants colonized by *S. indica*. Fading of nuclei at the onset of cell death during fungal colonization was regularly observed.

## RESULTS

### Fading of host nuclei and vacuolar collapse are hallmarks of symbiotic cell death during *S. indica* root colonization

*S. indica* induces restricted cell death in colonized root cells of Arabidopsis and barley, resulting in characteristic cytological features at later stages of colonization. In these two hosts, the timing and extent of cell death differ.[5,6] In Arabidopsis, the cell death phenotype is less pronounced than in barley, but cytological analyses showed fading of host nuclei, vacuolar collapse, and swelling of the endoplasmic reticulum (ER) in colonized cells,[5] indicating ER stress and host cell death during root colonization (Figures 1B–1N). To characterize the timing of fungal-induced cell death, the presence and shape of plant nuclei during colonization by *S. indica* were monitored by confocal laser scanning microscopy using either an Arabidopsis line expressing the nuclear marker H2B:mCherry (Figures 1B and 1C) or the nucleic acid dye DAPI (Figures 1D–1F) and the cell death dye SYTOX Orange (Figures 1G and 1H). In the Arabidopsis H2B:mCherry line, plant nuclei in the epidermal layer were often elongated (Figures 1B and 1C), faded, and eventually disappeared by 8 to 10 dpi in heavily colonized areas of the root. Nuclei stained with SYTOX Orange were visible at 7 to 8 days post inoculation (dpi), indicating that at this time the plasma and nuclear membranes of Arabidopsis were permeable to the dye, which is a hallmark of cell death (Figures 1G and 1H). In dying cells, *S. indica* hyphae embedded in plant nuclei were frequently observed, indicating that during activation of cell death, the fungus might digest and feed on host nuclear DNA (Figures 1E, 1F, 1I, and 1J). These results show that Arabidopsis root cell death begins around 7 dpi, and by 10 dpi, most host nuclei have faded or disappeared in cells colonized by *S. indica*.

### *Si*NucA and *Si*E5NT act synergistically in the production of deoxynucleosides

Although the interaction between *S. indica* and roots has been extensively studied, comparatively little is known about the contribution of apoplastic effectors to fungal accommodation or the mechanism of cell death in this system.[13,18,20,26] We previously analyzed soluble apoplastic proteins in barley at different stages of *S. indica* colonization. We found that *Si*E5NT was consistently one of the predominant fungal proteins.[13] We demonstrated that *Si*E5NT functions as a membrane-bound nucleotidase that is released into the apoplast during host colonization. Partially purified preparations of *Si*E5NT are capable of releasing phosphate and adenosine from ATP, ADP, and AMP.[13] In addition, the small secreted protein *Si*NucA with predicted endonuclease activity (Figure S1) was found in the apoplastic fluid of colonized barley roots at the onset of cell death (5 dpi).[13] *Si*NucA is also secreted during root colonization in Arabidopsis.[23] *Si*NucA expression is transiently induced during cell death in barley and Arabidopsis, as shown by transcriptomic data[6] and quantitative PCR analyses (Figure 2A). This prompted us to further investigate the involvement of *Si*NucA in fungal colonization and host cell death. The secretion of *Si*NucA and its enzymatic activity were investigated by overexpressing a *SiNucA*:HA:His construct in *S. indica* (Figures 2B and S1). Supernatants from fungal overexpression (OE) strains and affinity-purified *Si*NucA were able to degrade double-stranded DNA and single-stranded RNA from fungal and plant material, indicating nonspecific nuclease activity (Figure 2C). Addition of magnesium and calcium increased *Si*NucA activity in *in vitro* assays, whereas EDTA inhibited it (Figure S1F).

To investigate the effects of *Si*NucA on colonization, we tested independent homozygous T3 lines heterologously expressing a native version of *SiNucA* in Arabidopsis under control of the 35S promoter. Expression of *SiNucA* in Arabidopsis resulted in higher fungal colonization at 7 dpi, which correlated with the *SiNucA* expression level (Figures 2D and 2E), demonstrating its importance in fungal accommodation. Overcolonization resulted in a reduction in plant biomass that was not observed in the mock-treated *SiNucA* expression lines (Figure S2A). Localization studies by confocal microscopy of Arabidopsis roots expressing either full-length *Si*NucA or a version lacking the N-terminal signal peptide (SP) fused to mCherry confirmed secretion of the full-length *Si*NucA fusion protein into the apoplast and functionality of the SP. After plasmolysis, the mCherry fluorescence signal was visible on the cell walls and apparently on the membrane of the shrinking cells for the full-length *Si*NucA fusion protein but not for the cytoplasmic version without SP (Figures S2B and S2C). Remarkably, *S. indica* colonization was associated with the observation that the full-length mCherry-tagged *Si*NucA localized to host nuclei specifically in colonized cells. By contrast, in adjacent non-colonized cells, the mCherry signal was localized at the cell periphery, even following plasmolysis (Figures 2F and S2B–S2D). The detection of *Si*NucA in the apoplast[13] and within the nuclei of colonized host cells (Figure 2F) suggests that it may be directed toward the nucleus during colonization, where it could potentially interact with both eDNA and nuclear DNA.

The co-occurrence of *Si*NucA and *Si*E5NT in the apoplast at 5 dpi led us to speculate that these two enzymes might cooperate in promoting fungal colonization of roots. Using affinity-purified *Si*E5NT from leaves of *Nicotiana benthamiana*, we found activity with dAMP and AMP substrates (Figures 3A and 3B), whereas no activity was detected for other deoxynucleotides (deoxycytidine monophosphate, deoxyguanosine monophosphate, deoxythymidine monophsophate) or nucleotides (guanosine monophosphate, uridine monophosphate, 3′,5′-cAMP) tested. Moreover, dATP and the general phosphatase substrate *para*-nitrophenyl pyrophosphate (pNPP) were not *Si*E5NT substrates. Interestingly, only dAMP was hydrolyzed at a constant rate, whereas the AMP hydrolysis rate gradually decreased under the selected reaction conditions (Figures S3A and S3B). The $K_M$ for AMP (15.9 μM) was ~20-fold lower than for dAMP (361.6 μM), but the $k_{cat}$ for dAMP (11.9 $s^{-1}$) exceeded that of AMP (1.1 $s^{-1}$) by a factor of ~10 (Figures 3A and 3B). These data suggest that *Si*E5NT hydrolyzes AMP slightly better at low substrate concentrations (below 20 μM) but is far more efficient for dAMP at higher substrate concentrations that might prevail in a nucleus undergoing degradation and in the case of eDNA degradation. To test potential synergistic activity of *Si*NucA and *Si*E5NT, we incubated DNA with *Si*E5NT and *Si*NucA alone and in combination. As expected, *Si*NucA degraded DNA (Figure 3C), but neither deoxynucleotides nor deoxynucleosides were detected as reaction products by LC-MS analysis, suggesting that *Si*NucA degrades DNA to oligonucleotides. *Si*E5NT also did not release deoxynucleotides from DNA but produced small amounts of

CellPress
OPEN ACCESS

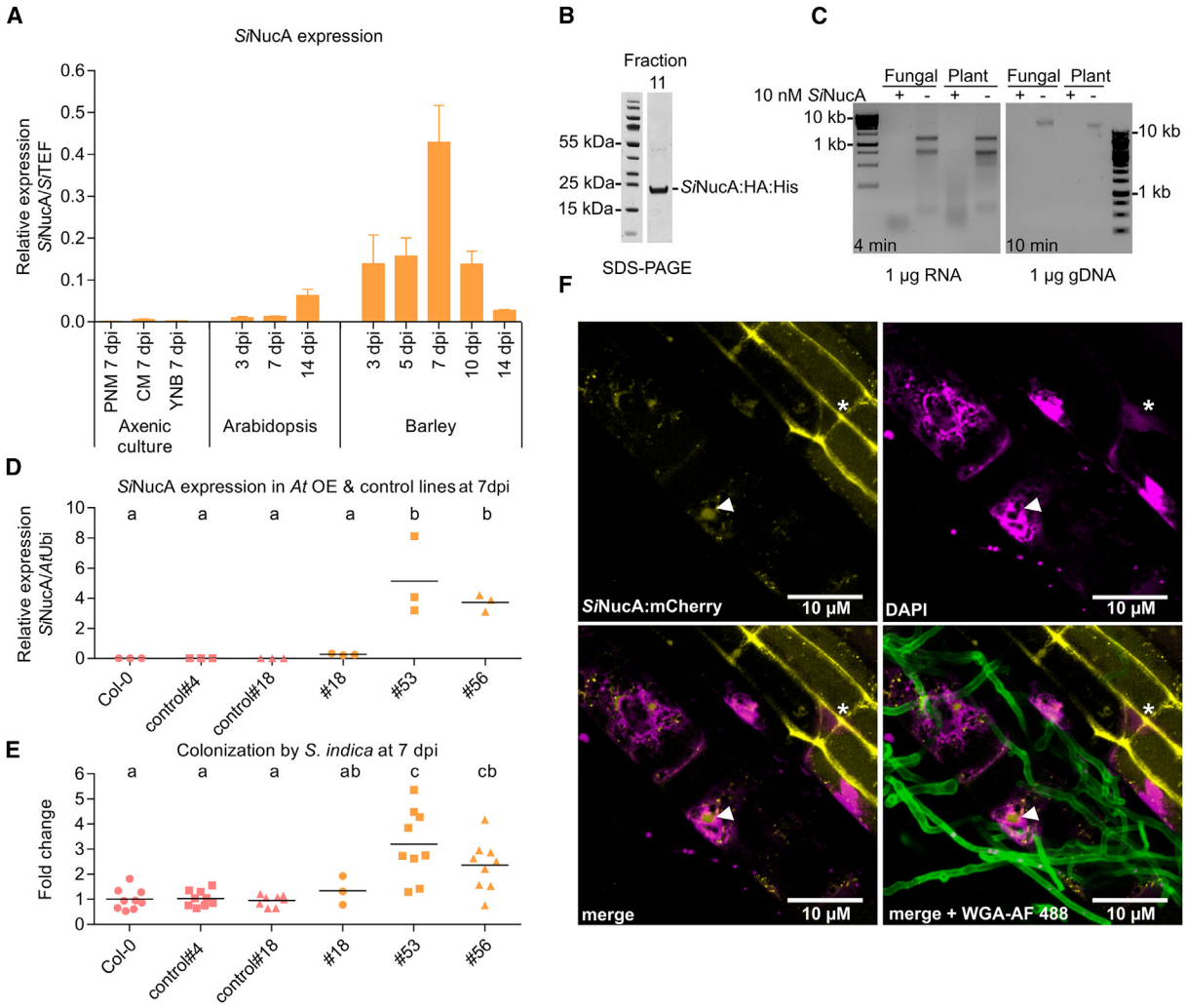


**Figure 2. *Si*NucA is a small secreted nuclease involved in fungal accommodation**

(A) *Si*NucA expression in Arabidopsis and barley roots colonized by *S. indica* and axenic cultures measured by the $2^{-\Delta CT}$ method. Error bars: SD, $n = 3$ (biological replicates).

(B) *Si*NucA:HA:His protein enrichment from culture filtrate precipitated with 80% ammonium sulfate and separated by size exclusion chromatography. The resulting fraction was separated by SDS-PAGE, and *Si*NucA:HA:His was stained with Coomassie brilliant blue.

(C) The purified *Si*NucA:HA:His protein was incubated with fungal (*S. indica*) or plant (Arabidopsis) RNA or DNA in 5 mM Tris buffer (pH = 8) containing 1 mM $MgCl_2$ and 1 mM $CaCl_2$ for 4 (RNA) or 10 (DNA) min and visualized after gel electrophoresis.

(D) Arabidopsis lines expressing *SiNucA* driven by the 35S promoter (lines 18, 53, and 56) compared with control lines (4 and 18: segregating from T2 generation and Col-0 WT). Roots of plants grown on ½ MS medium were inoculated with *S. indica* and analyzed after 7 dpi. The dots represent independent biological replicates, and the lines represent the mean. Different letters indicate significantly different groups as determined by one-way ANOVA with post-hoc Tukey HSD test ($p < 0.05$).

(E) Root colonization by *S. indica* in transgenic 35S::*SiNucA*-Arabidopsis lines at 7 dpi was assessed by RT-qPCR by comparing expression of the fungal housekeeping gene *SiTEF* and the plant gene *AtUbi* and the $2^{-\Delta\Delta CT}$ method, normalized to colonization in the WT Col-0. The dots represent independent biological replicates, while the lines represent the mean. Different letters indicate significantly different groups as determined by one-way ANOVA with post-hoc Tukey HSD test ($p < 0.05$).

(F) CLSM live cell images of an Arabidopsis root expressing *Si*NucA:mCherry (yellow) and inoculated with *S. indica*. Fungal cell walls are stained with WGA-AF 488 (green) and nuclei with DAPI (magenta). *Si*NucA:mCherry fluorescence signal accumulates in the apoplast/cell periphery in non-colonized root cells (asterisk) and (re)localizes in host nuclei in colonized cells (arrow).

deoxynucleosides (Figure 3D). However, in combination, *Si*NucA and *Si*E5NT released deoxynucleosides from DNA with a strong preference for dAdo. This demonstrates the ability of *Si*E5NT to use oligonucleotides released by *Si*NucA as a substrate and act synergistically with *Si*NucA to preferentially release dAdo from DNA (Figure S3C).

## dAdo induces host cell death

The production of dAdo by the synergistic activity of the two secreted fungal enzymes resembles the processes involved in dAdo-mediated immune cell death of *S. aureus* in animal cells, which ensures the exclusion of macrophages from the center of abscesses where the bacteria survive.[24,25] This motivated

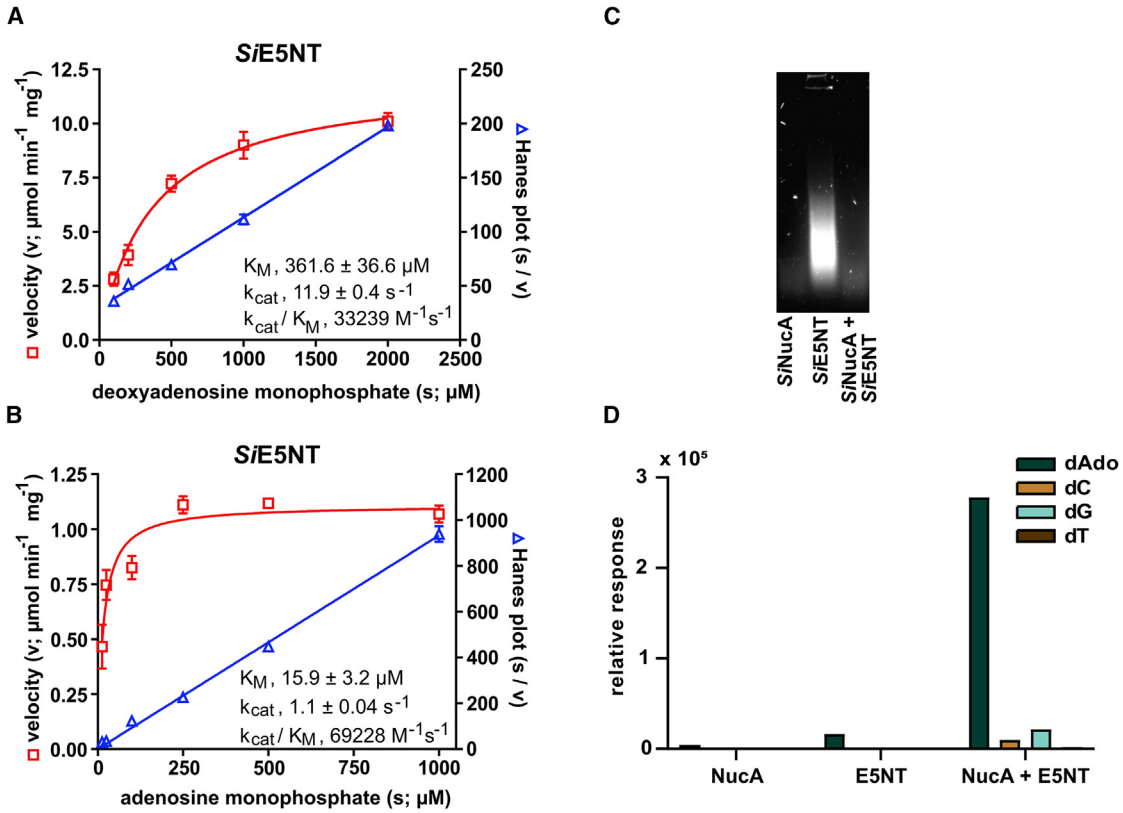


**Figure 3. *Si*NucA and *Si*E5NT act synergistically in the production of deoxy nucleosides from DNA**

(A) Enzymatic activity and kinetic constants of *Si*E5NT. Left axis, initial catalytic velocity (v) for phosphate production at different dAMP concentrations fitted with the Michaelis-Menten equation. Right axis, ratio of dAMP concentrations and velocities (s/v) plotted against dAMP concentrations (s) fitted by linear regression (Hanes plot). Error bars: SD, $n = 3$.

(B) As in (A), but using AMP as substrate ($n = 3$).

(C) Degradation of DNA by *Si*NucA and/or *Si*E5NT. 2% agarose gel loaded with the products of a 1-h incubation of 10 µg salmon sperm DNA at 25°C with different enzyme combinations. (D) Relative quantification of deoxyadenosine (dAdo), deoxycytidine (dC), deoxyguanosine (dG), and deoxythymidine (dT) released during incubation in (C) by HPLC-MS/MS. Deoxynucleotides could not be detected in any of the reactions.

us to test the effect of dAdo in plants. Incubation of the Arabidopsis H2B-mCherry line with extracellular dAdo but not with Ado resulted in the fading and disappearance of nuclei in roots within 48 h (Figure 4A). This root cell death phenotype could be quantified using Evans blue azo dye (Figures 4B and 4C). In addition, extracellular dAdo-triggered hallmarks of cell death, such as increased electrolyte leakage, induction of cell death marker gene expression, as well as activation of the 26S proteasome, and decreased photosynthetic activity ($F_V/F_M$) (Figures 4D–4H and S4A). The effects were concentration-dependent, and removal of dAdo from the culture supernatant 24 h post treatment (hpt) resulted in recovery of Arabidopsis seedlings, indicating that activation of this cell death program is still reversible at this stage (Figures S4B and S4C).

A cell death phenotype was also observed in young leaves of *N. benthamiana* during expression by *Agrobacterium tumefaciens* infiltration of a *SiE5NT* construct, including the SP for secretion (Figure S5) and in seedlings incubated with dAdo (Figure S6A). Cell death was not visible in older leaves or in leaves of *N. benthamiana* expressing *SiNucA* or the suppressor of gene silencing p19. The observed phenotype suggests that the presence of *Si*E5NT is sufficient to trigger cell death in this plant host upon wounding by agroinfiltration, which could release DNA and DNases into the apoplast or elicit a response to the presence of the bacterium or its proteins. To test whether cell death triggered by dAdo is conserved in basal plant lineages, we additionally tested its effect on the liverwort *Marchantia polymorpha*. Incubation with dAdo also induced cell death in this plant species (Figure S6B). These findings suggest that dAdo-mediated cell death operates through a conserved mechanism across diverse plant lineages. However, the precise extent and regulatory pathways involved in different species require further investigation.

## dAdo induces the MEP pathway and accumulation of the stress-signaling metabolite MEcPP

To investigate the mechanism by which dAdo triggers cell death in plants and to determine whether it activates stress-signaling pathways, we analyzed the transcriptional response of Arabidopsis at 0, 3, and 12 hpt using RNA-seq. Most marker genes for RCD [28] were upregulated at 12 h (Figure 4I; Tables S1, S2, and S3). In addition, the plastidial 2-C-methyl-D-erythritol-4-phosphate (MEP) pathway was induced at 12

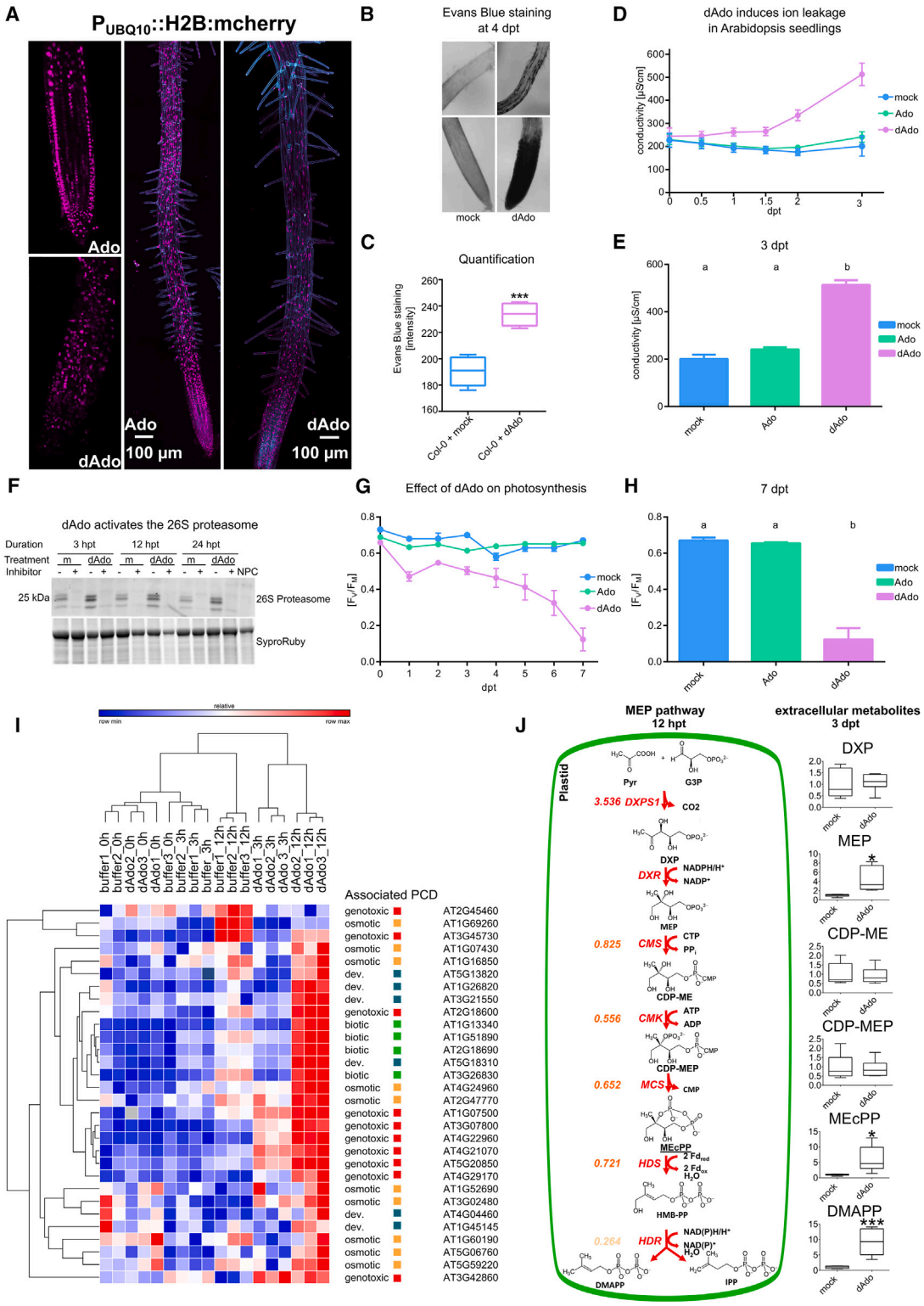


**Figure 4. dAdo induces cell death *in planta***

(A) CLSM images of 7-day-old Arabidopsis roots expressing the nuclear marker UBQ10::H2B:mCherry. Incubation with dAdo but not Ado (500 µM) results in disorganization of Arabidopsis cells in the root tip and disappearance or fading of nuclear material.

(B) Bright-field microscopy of the root tip and differentiation zone of Arabidopsis seedlings treated with mock/dAdo (500 µM) and stained with Evans blue cell death dye.

*(legend continued on next page)*

hpt (Figure 4J; Table S4). Accordingly, MEcPP, a precursor of plastidial isoprenoids and a stress-specific retrograde signaling metabolite produced by the MEP pathway, accumulated extracellularly 3 days post treatment (dpt) as measured by liquid chromatography-tandem mass spectrometry (LC-MS/MS) (Figure 4J). Abiotic stress and wounding increase levels of cytoplasmic MEcPP, which coordinates stress response pathways in plants.[29] The detection of this isoprenoid intermediate in the extracellular environment after dAdo treatment suggests that this metabolite may serve as a stress signal in bystander cells. Incubation of Arabidopsis with extracellular MEcPP did not result in cell death, demonstrating that accumulation of this metabolite is not sufficient to trigger cell death and therefore is not the cause of the observed dAdo-mediated cell death (Figure S6C).

## dAdo-triggered signaling and cell death are not mediated by canonical pattern-triggered immune responses

To determine whether cell death triggered by dAdo is mediated by signals generated by an immune receptor at the cell surface, we tested the ability of it to trigger a rapid response by monitoring calcium influx and ROS production. Both responses are part of pattern-triggered immunity (PTI), a process activated by recognition of microbe-associated molecular patterns (MAMPs) or damage-associated molecular patterns (DAMPs) by pattern-recognition receptors (PRRs) at the plasma membrane.[30–32]

Incubation of Arabidopsis seedlings with dAdo did not elicit calcium influx, whereas treatment with ATP or ADP, which have been previously described as DAMPs[33,34] but also with dATP or dADP, triggered a rapid calcium influx that was dependent on the eATP receptor P2K1/DORN1 (Figures S7A–S7C). Treatment with dAdo or with any of the other purine derivatives did not induce a ROS burst (Figures S7F and S7G). On the other hand, incubation with dAdo and to a lesser extent with ATP or dAMP but not Ado resulted in accumulation of the stress marker metabolite MEcPP and induction of the DAMP/MAMP- and fungus-responsive gene AT1G58420 at 3 dpt (Figures S7D and S7E; Table S5).[13,33,35] Overall, these data suggest that dAdo does not act as a typical extracellular DAMP or MAMP but induces a signaling pathway independent of calcium influx and ROS production.

## The Arabidopsis transporter ENT3 is required for dAdo-mediated signaling and cell death

The fact that we did not observe a canonical PTI response to dAdo led us to speculate that uptake of this metabolite is necessary to promote plant signaling and trigger cell death. In the animal system, treatment with extracellular dAdo leads to the accumulation of intracellular dATP, which appears to impair DNA synthesis and induces apoptosis via activation of caspase 3.[25] Rapidly dividing cells are particularly susceptible to cell death triggered by dAdo, and it has been shown that the toxic effect of dAdo in the animal system depends on dAdo uptake by the human ENT1 (hENT1).[25] Similarly, we observed high sensitivity of dividing cells in root tips using Evans blue staining and young *N. benthamiana* plants (Figures 4A, 4B, and S6A). On the contrary, *S. indica* was not sensitive to dAdo and showed normal growth even at high concentrations (Figure S8). In Arabidopsis, eight potential ENT family members are annotated in the genome. Two of them are expressed in roots, namely ENT3, which is localized at the plasma membrane, and ENT1, which is localized at the tonoplast. The Arabidopsis KO line *ent3* showed a stronger resistance phenotype to dAdo-induced cell death compared with both the WT and *ent1* KO lines but is unaffected in the response to MeJA-induced cell death (positive control) (Figures 5A–5C and S9A–S9E). ENT3 has been shown to transport adenosine and uridine with high affinity, and their uptake is competitively inhibited by co-treatment with various purine and pyrimidine nucleosides and 2′-deoxynucleosides, including dAdo.[36] This suggests that ENT3 has a broad substrate specificity and is a strong candidate for uptake of extracellular dAdo. In a competition assay, addition of extracellular Ado decreased the cell death phenotype induced by dAdo, suggesting that these two extracellular metabolites compete for the same transporter at the cell membrane (Figure 5D). Interestingly,

(C) Quantification of root cell death in Col-0 root tips 4 days after dAdo treatment. Cell death was assessed by Evans blue staining. Boxplots show data from 5 biological replicates. Asterisks represent a significant difference from the mock-treated samples analyzed by Student's t test ($p < 0.005$ ***). The experiment was independently repeated 3 times with similar results.
(D) Electrolyte leakage of Col-0 seedlings (9 days old) in MES buffer after mock, Ado, or dAdo treatment. Error bars show the standard error of the mean (SEM) from 6 biological replicates. The experiment was independently repeated at least 3 times with similar results.
(E) Electrolyte leakage at 3 dpt of seedlings from (D). Error bars show the SEM of 6 biological replicates. Different letters indicate significantly different groups as determined by one-way ANOVA with post-hoc Tukey HSD test ($p < 0.05$). The experiment was independently repeated at least 3 times with similar results.
(F) Activity of the 26S proteasome of Arabidopsis. Total protein extracts from 14-day-old seedlings treated with 500 μM dAdo or 2.5 mM MES buffer (M) were incubated with 1 μM of probe MVB072.[27] Prior to labeling, samples were incubated with 50 μM of the proteasome inhibitor epoxomicin (+) or DMSO (−). Samples were then labeled for 2 h and separated by SDS-PAGE. 26S proteasome activity was visualized by fluorescence scanning. SYPRO™ Ruby staining was performed to compare sample amounts. A non-probe control (NPC) consisting of a mixture of all samples incubated with DMSO was used as an additional control. The experiment was repeated twice with similar results.
(G) Photosynthetic activity ($F_V/F_M$) of 7-day-old Col-0 seedlings incubated with 500 μM Ado or dAdo. Error bars represent the SEM obtained from twelve biological replicates. The experiment was repeated three times with similar results.
(H) Photosynthetic activity ($F_V/F_M$) of 7-day-old Col-0 seedlings incubated with 500 μM Ado or dAdo at 7 dpt from (G). Error bars represent the SEM obtained from twelve technical replicates. Different letters indicate significantly different groups as determined by one-way ANOVA with post-hoc Tukey HSD test ($p < 0.05$).
(I) Heatmap of core regulated cell death (RCD) marker-genes expression (selected from Olvera-Carrillo et al.[28]) of 7-day-old Arabidopsis seedlings after dAdo treatment at 0, 3, and 12 h. RNA-seq data are presented as $\log_2$ (tpm) (Table S6). Heatmaps and hierarchical clustering (one-minus Pearson correlation) were generated using Morpheus, https://software.broadinstitute.org/morpheus.
(J) Graphical representation of the methyl erythritol 4-phosphate (MEP) pathway. The colored numbers on the left represent the $\log_2$ fold-change after 12 h of dAdo treatment ($padj < 0.05$) as measured by RNA-seq. The boxplots on the right show the corresponding extracellular metabolites at 3 dpt. Asterisks represent significant differences from the mock-treated sample analyzed by Student's t test (*$p < 0.05$; ***$p < 0.001$).

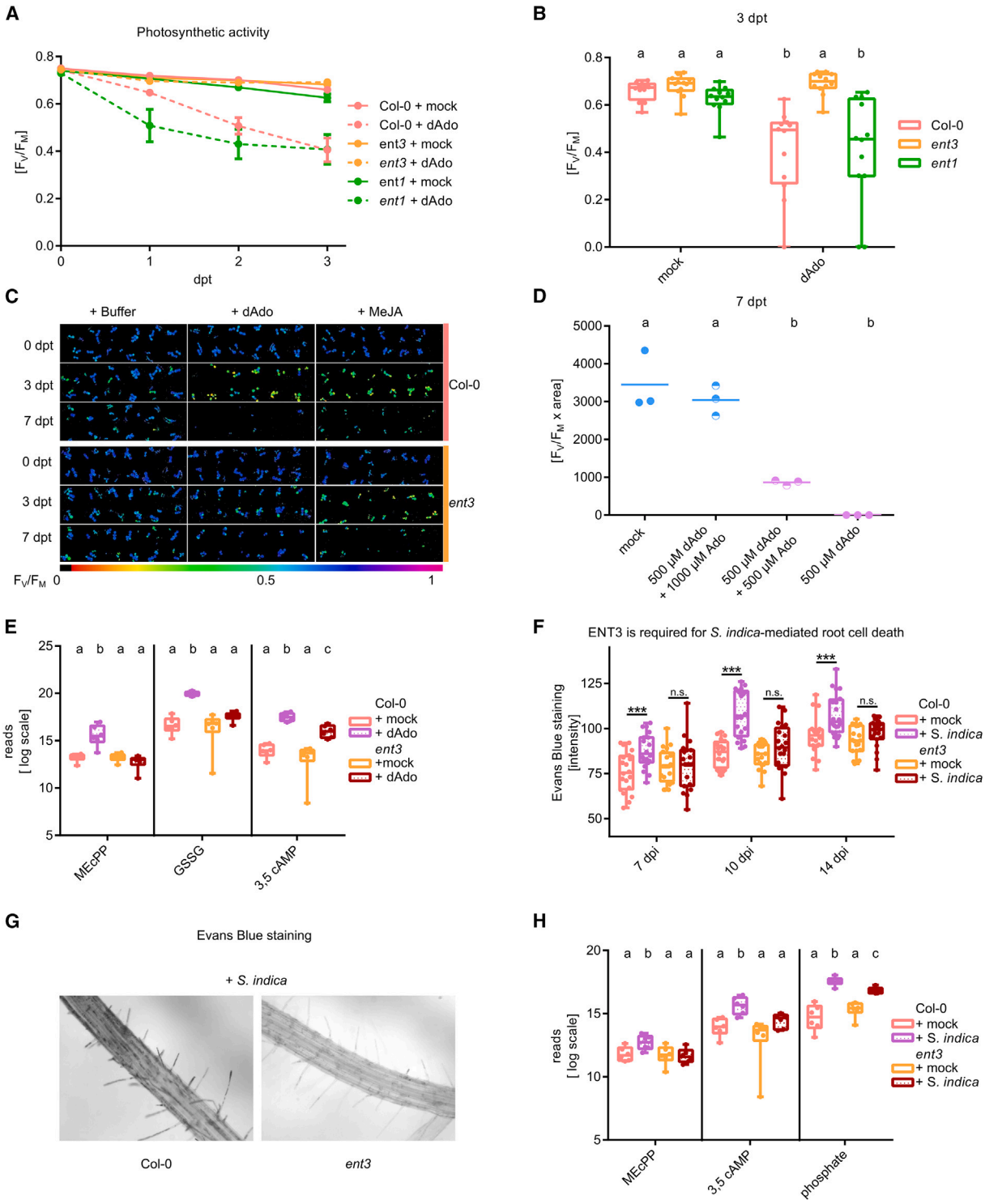


**Figure 5. The equilibrative nucleoside transporter ENT3 of Arabidopsis is required for dAdo-mediated signal transduction and cell death**

(A) Photosynthetic activity ($F_V/F_M$) of 9-day-old mock- and dAdo-treated (500 µM) Col-0, *ent3*, and *ent1* seedlings. Measurements were taken 3 days after treatment (dpt) every 24 h. Data show the mean, and error bars show the SEM obtained from 12 technical replicates with 3 seedlings each. The experiment was repeated more than three times independently with similar results.

(B) $F_V/F_M$ of seedlings from (A) at 3 dpt. Boxplots show data from 12 technical replicates with 3 seedlings each. Different letters indicate significant differences as determined by one-way ANOVA with post-hoc Tukey HSD test ($p < 0.05$).

*(legend continued on next page)*

ENT3 is expressed at higher levels in the epidermis compared with the rest of the root,[37] suggesting that dAdo-induced cell death may be cell-type specific to some extent. This is consistent with the phenotype of root cell death observed after dAdo treatment with Evans blue staining (Figures 4B and 4C). Taken together, these data indicate that a functional ENT3 plays an important role in dAdo-triggered cell death in Arabidopsis, most likely by importing dAdo into the cytoplasm, where it activates signaling leading to cell death. Accordingly, the *ent3* KO line accumulates lower levels of extracellular signaling metabolites such as MEcPP, GSSG, and 3′,5′-cAMP in response to dAdo at 3 dpt compared with the WT line (Figure 5E; Table S6).

## Mutation of *ENT3* impairs *S. indica*-mediated cell death

Next, we investigated whether ENT3 plays a role in fungal accommodation and cell death mediated by *S. indica* in roots. The *ent3* line showed significantly less cell death upon colonization by *S. indica* compared with the WT line at 7, 10, and 14 dpi (Figures 5F and 5G). In addition, we observed a transient effect on fungal colonization at 8 dpi, where the *ent3* KO line was less colonized by *S. indica* compared with the WT control (Figure S9F).

Colonization with *S. indica* also resulted in transient accumulation of the extracellular signaling metabolites 3′,5′-cAMP at 3 dpi (early biotrophic phase) and MEcPP at 6 dpi (onset of cell death). In addition, a higher level of free phosphate was observed at 10 dpi (Figure 5H; Table S6). Consistent with the decreased cell death phenotype in the *ent3* KO line, the amount of these metabolites was lower in colonized *ent3* seedlings, suggesting that ENT3 is important for fungal-mediated signal transduction and cell death in Arabidopsis. The activity of the fungal-derived enzymes *Si*NucA and *Si*E5NT, along with the host transporter ENT3, modifies extracellular metabolite levels, establishing for the first time a direct link between purine metabolism, immunity, and cell death in roots. How the metabolic state of the host affects *S. indica*-induced cell death remains to be thoroughly elucidated.

## Screening of Arabidopsis T-DNA insertion mutants reveals a TIR-NLR gene involved in dAdo-mediated cell death

To identify downstream genetic determinants associated with dAdo-mediated cell death in plants, we performed a mutant screen of 6,868 SALK-Arabidopsis T-DNA insertion lines (Figure S10A). Sensitivity to dAdo was tested using Arabidopsis Col-0 WT as control and the SALK mutant lines grown for 14 days on solid media (½ MS) in 24-well plates with and without 500 μM dAdo. The dAdo-insensitive lines (survivors) from the screening were then analyzed by pulse amplitude modulation (PAM) fluorometry in three independent biological replicates. Thirteen lines with varying degrees of dAdo resistance were identified (Table S7). One of the resistant SALK lines had an insertion at the AT5G45240 locus (SALK_034517C), which encodes a predicted TIR-domain NLR (TIR-NLR). Mutation in this locus resulted in reproducible and significantly high resistance to dAdo-induced cell death, as evidenced by reduced electrolyte leakage, higher photosynthetic activity, and increased germination rate compared with Col-0 WT after incubation with dAdo (Figure 6). No differences were observed in response to the cell death inducer MeJA (Figure S10B). An independent KO line, *CRISPRisi*, generated using a CRISPR-CAS9-based approach (Figure S11A)[38,39] and carrying two indel mutations in the TIR domain (Figure S11B), also exhibited a dAdo-resistant phenotype (Figures S11C and S11D), further supporting a connection between this locus and dAdo-mediated cell death. Complementation using a cell-based transient expression system with the full-length TIR domain restored sensitivity to dAdo, suggesting that the TIR domain may play a role in mediating dAdo-induced cell death in Arabidopsis (Figure 6E). The TIR-NLR gene AT5G45240 is located in close proximity to *RPS4* and *RRS1* and is part of a larger locus containing multiple TNL genes, most of which are functionally uncharacterized. Four of the five TNL genes at this locus showed transiently increased expression during cell death associated with colonization by *S. indica*, with the AT5G45240 gene displaying the strongest relative induction (Figures S12A and S12B). We therefore named this gene *ISI*, induced by *S. indica*. Induction could be detected, especially during the onset of the cell death-associated phase (Figure 7A). While the *isi* line showed less cell death after dAdo treatment (Figure S12C), there was increased cell death in the older parts of the mock-treated roots and during colonization with *S. indica* compared with the WT line (Figure 7B), which correlated with significantly greater fungal colonization (Figure 7C). In addition, colonized *isi* KO seedlings did not show *S. indica*-mediated promotion of root growth, as observed in WT and *ent3* seedlings (Figures 7D and S12D). These results could be explained by the activation of an alternative cell death

(C) Visualization of $F_V/F_M$ measured by PAM fluorometry. The $F_V/F_M$ value is visualized by the color scale shown below. Shown are 12 wells with 9-day-old seedlings probed at 0, 3, and 7 dpt with either mock treatment (2.5 mM MES buffer pH 5.6), 500 μM dAdo, or 500 μM MeJA. The experiment was repeated more than three times independently with similar results.

(D) Photosynthetic activity ($F_V/F_M$ × photosynthetically active area) of 9-day-old Col-0 seedlings incubated with different concentrations of Ado and dAdo at 7 dpt. Dots represent 3 biologically independent replicates consisting of 12 wells with 3 seedlings each. Different letters indicate significant differences as determined by one-way ANOVA with post-hoc Tukey HSD test ($p < 0.05$).

(E) Metabolic analysis of supernatants from 7-day-old Col-0 and ent3 seedlings treated with dAdo at 3 dpt. Boxplots show data from 6 biologically independent replicates. Data are plotted on a $\log_2$ scale. Different letters indicate significant differences in measurements of a metabolite as determined by two-way ANOVA with post-hoc Tukey HSD test ($p < 0.05$).

(F) Quantification of root cell death in 7-day-old Col-0 and *ent3* roots colonized with *S. indica* at 7, 10, and 14 dpi. Cell death was assessed by Evans blue staining. Boxplots show data from 20 biological replicates. Asterisks represent significant differences analyzed by Student's t test (*$p < 0.05$, **$p < 0.01$, ***$p < 0.005$). The experiment was repeated independently three times with similar results.

(G) Evans blue staining of *S. indica*-colonized Col-0 and *ent3* roots at 10 dpi.

(H) Metabolic analysis of the supernatant of 7-day-old Col-0 and *ent3* seedlings inoculated with *S. indica* at different time points after treatment (3′,5′-cAMP: 3 dpi; MEcPP: 6 dpi; phosphate: 10 dpi). Boxplots show data from 6 biologically independent replicates. Data are plotted on a $\log_2$ scale. Different letters indicate significant differences in measurements of a metabolite using a two-way ANOVA with post-hoc Tukey HSD test ($p < 0.05$).

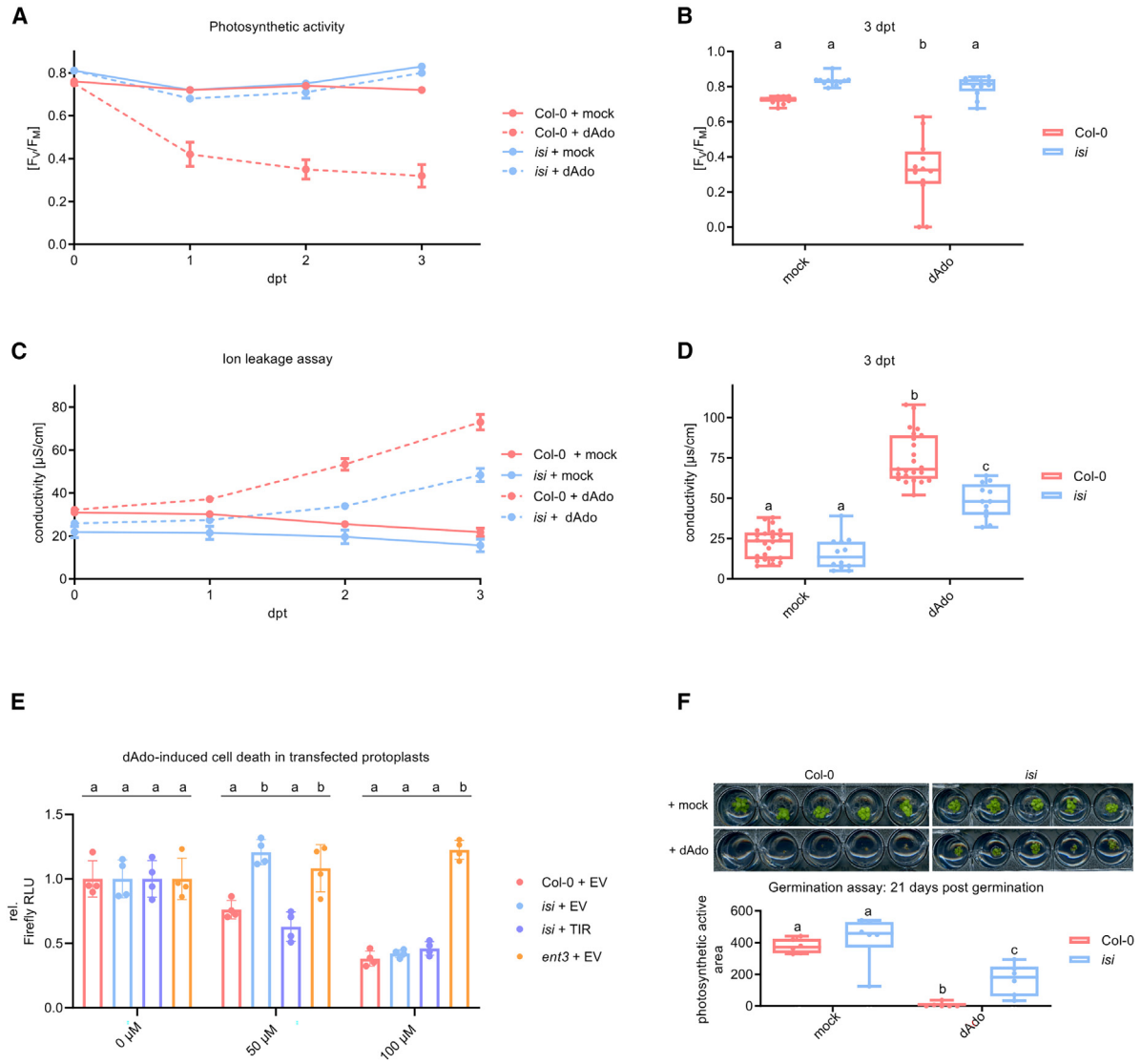


**Figure 6. The *At*TIR-NLR AT5G45240 is involved in dAdo-mediated cell death**

(A) $F_V/F_M$ of 9-day-old mock- and dAdo-treated (500 µM) Col-0 and *isi* (AT5G45240 KO mutant) seedlings. Measurements were performed over 3 days. Data show the mean, and error bars show the SEM obtained from 12 technical replicates with 3 seedlings each. The experiment was repeated three times independently with similar results.

(B) Boxplots of the measurements of $F_V/F_M$ from (A) at 3 dpt. Different letters indicate significant differences as determined by two-way ANOVA and post-hoc Tukey HSD test ($p < 0.05$).

(C) Conductivity of water containing 9-day-old Col-0 or *isi* seedlings 0–3 days after mock or dAdo treatment (500 µM). Data points represent the mean, while error bars show the SEM from 12 biological replicates.

(D) Boxplots of conductivity measurements from (C) at 3 dpt. Different letters indicate significant differences as determined by two-way ANOVA with post-hoc Tukey HSD test ($p < 0.05$).

(E) Relative luciferase activity of *A. thaliana* protoplasts transfected with luciferase and either a construct expressing the TIR domain of ISI or an empty vector. Values were normalized to mock treatment (0 µM dAdo). Different letters indicate significantly different groups per treatment, as determined by one-way ANOVA with post-hoc Tukey HSD test ($p < 0.05$).

(F) Germination of Col-0 WT and *isi* seedlings on 1/10 PNM medium containing 500 µM dAdo or MES. The upper half shows photographs of the seedlings after 21 days. The lower half shows the quantification of $F_V/F_M$ measured by PAM fluorometry. Boxplots show $F_V/F_M$ measurements per well, containing six seedlings. Different letters indicate significant differences as determined by two-way ANOVA with post-hoc Tukey HSD test ($p < 0.05$). The experiment was repeated three times independently with similar results.

pathway in the absence of a functional ISI TIR-NLR, leading to overcolonization by *S. indica* and loss of growth promotion (Figure 7E). Overall, our data suggest that the ISI TIR-NLR protein is involved in modulating different cell death programs in roots and mediating *S. indica* growth promotion. We further analyzed the expression of both TIR- and CC-NLRs in the roots of Arabidopsis

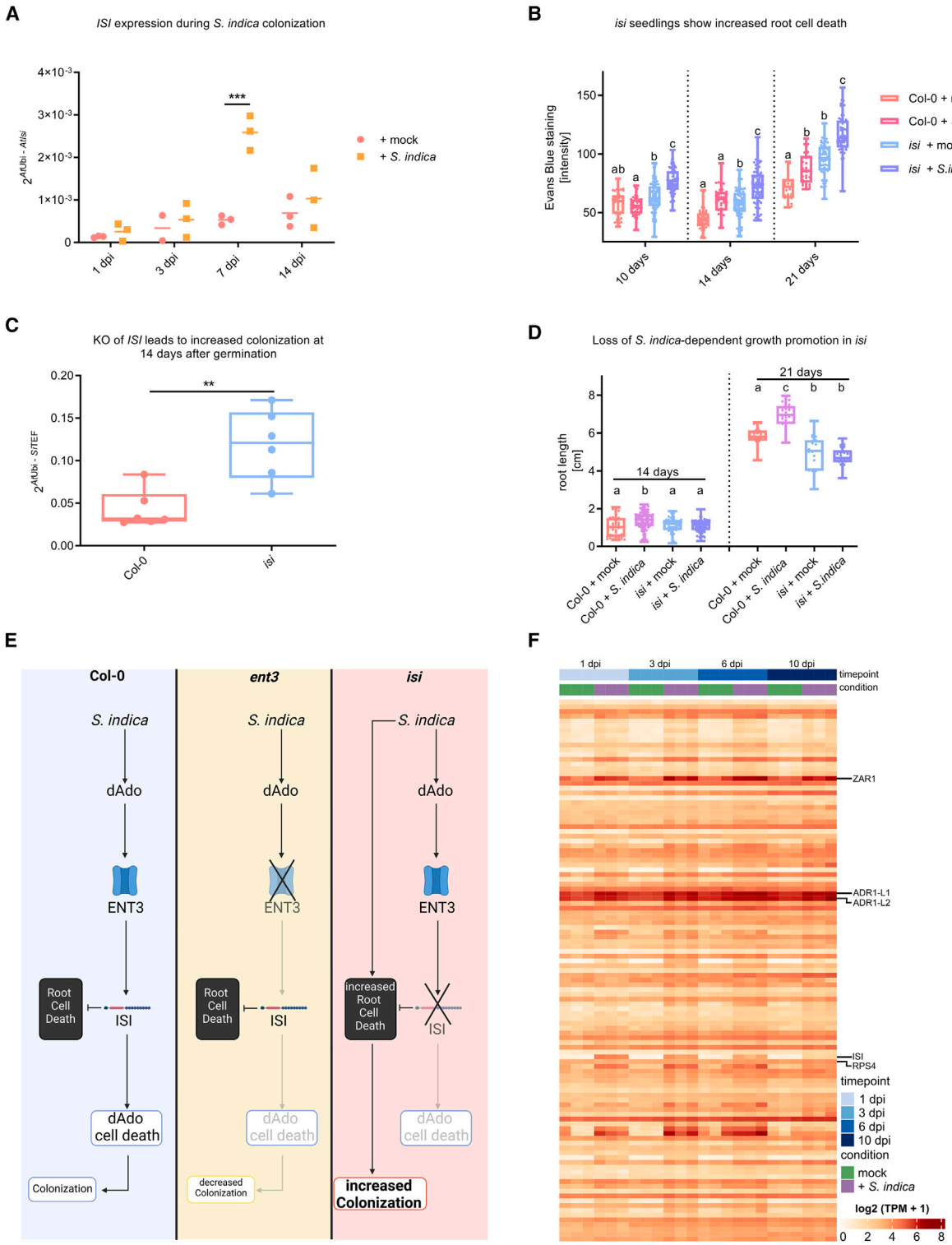


**Figure 7. The *At*TIR-NLR AT5G45240 is involved in fungal-mediated growth promotion**

(A) AT5G45240 *(AtISI)* expression in Arabidopsis roots inoculated with *S. indica* or mock treated. Expression was measured via RT-qPCR and calculated with the $2^{-\Delta CT}$ method. Data points depict biological replicates, and asterisks represent significant differences analyzed by Student's t test (***$p < 0.005$).

(B) Quantification of root cell death in Col-0 WT and *isi* roots colonized by *S. indica* at 10, 14, and 21 days after germination. Cell death was assessed by Evans blue staining. Boxplots show data from 28–80 biological replicates. Different letters indicate significant differences between samples from one time point as assessed by two-way ANOVA with post-hoc Tukey HSD test ($p < 0.05$).

*(legend continued on next page)*

during *S. indica* colonization using time-resolved transcriptomics. We detected an induction of expression for *ISI* and also for previously functionally characterized NLRs such as *ZAR1* during beneficial colonization (Figures 7F and S13). Overall, the role of a TIR-NLR in dAdo-induced cell death suggests that this cell death is influenced by the plant immune response and is not a pure consequence of cytoplasmic toxicity, as assumed for animal cells.

## DISCUSSION

### Symbiotic cell death: An evolutionarily conserved mechanism?

Root colonization by *S. indica* is associated with restricted host cell death. The mechanisms behind the induction and regulation of this symbiotic cell death are poorly understood. Previous work has shown that *S. indica* secretes *Si*E5NT, a ubiquitous apoplastic fungal enzyme that catalyzes the conversion of adenosine nucleotides released from immune-activated or damaged host tissues to adenosine.[13] The mechanism of the secreted ecto-5′-nucleotidase for host colonization appears to be similar to that evolved by *S. aureus* to evade the host immune response by secreting AdsA, which converts AMP to Ado, a suppressor of immunity in animal cells.[41] In addition to the release of eATP by damaged animal cells, activated neutrophils release NETs, extracellular matrices composed of nuclear and mitochondrial DNA and equipped with granular proteins, cell-specific proteases, and antimicrobial peptides.[42] NETs rapidly immobilize and kill bacterial pathogens.[43] *S. aureus* escapes NETs by secreting proteases and the nuclease Nuc, which degrade antimicrobial peptides and DNA. Nuclease-mediated degradation of neutrophil NETs results in the formation of dAMP, which is converted to dAdo by *S. aureus* AdsA. Macrophages and other immune cells are highly sensitive to dAdo. This cellular intoxication is mediated by uptake via ENTs.[24,25] The escape mechanism of *S. aureus* relies on the interaction of two extracellular microbial enzymes and allows staphylococci to block infiltration of abscess lesions by phagocytes and subsequent elimination. Similar to neutrophils, plant roots secrete root extracellurar traps (RETs) composed of eDNA and a variety of antimicrobial compounds and polysaccharides. RETs and NETs share similar compositional and functional properties, but unlike NETs, RET production is not triggered only upon microbial infection; instead, RETs are continuously released during root development and form a large, mucus-rich network in the rhizosphere.[43–46] By cytological analyses, we observed that *S. indica* is able to grow within RETs and along the root tip (Figure S14). The ability of *S. indica* to digest DNA via secretion of the nuclease NucA[13] suggests the possibility of RET digestion by *S. indica* during colonization. Moreover, localization of NucA in the nuclei of plant cells during *S. indica* colonization shows that this enzyme is able to digest host nuclear and eDNA. The combined enzymatic activity of *Si*E5NT and *Si*NucA, present simultaneously in the apoplast, results in the conversion of oligonucleotides with terminal dAdo obtained by nuclease digestion of DNA to free dAdo. Most importantly, we demonstrated that uptake of dAdo via ENT3 is required for host cell death in roots. Mutation of ENT3 results in reduced cell death during colonization by *S. indica*, demonstrating the importance of extracellular nucleoside uptake in regulating fungal-induced cell death. The identification of a previously unknown immune-metabolic axis by which cells respond to extracellular purine nucleosides and trigger cell death in plants suggests some conservation or functional convergence between the immune avoidance and escape mechanisms developed by *S. aureus* and other bacterial pathogens in animals and the cell death triggered by dAdo during plant-fungal endophyte interactions in roots.

### A TIR-NLR regulates host cell death in roots

To fight off infections by microbial pathogens, plants have evolved immune receptors that are essential for a successful defense response. PRRs localized in the plasma membrane are capable of sensing conserved MAMPs/DAMPs and eliciting a relatively mild PTI immune response. Successful plant-associated microbes can provide a range of effectors to attenuate PTI to enable successful host colonization. In turn, plants have evolved polymorphic intracellular resistance proteins (R-proteins) to recognize the presence and/or activity of effectors, resulting in a robust defense response called effector-triggered immunity (ETI) that potentiates PTI.[31,32] Most R-proteins belong to the nucleotide-binding (NB) leucine-rich repeat (LRR) family (NLR), which are classified on the basis of their N-terminal domains as TIR-type NLRs (TNLs) or coiled-coil type NLRs (CNLs).[47] TNLs generally function as sensors for microbial effectors, whereas several CNLs are referred to as helper NLRs and are downstream of many sensor NLRs in Arabidopsis.[47,48] TNL sensing and signaling mechanisms have primarily been studied in leaf cells, leaving much to be discovered about their function in roots, including which specific TNLs are involved.[49] The role of the TNL ISI in resistance to dAdo-mediated cell death in Arabidopsis suggests that this TIR-NLR or a potential interaction partner might guard a protein targeted by dAdo in the roots. Alternatively, dAdo might serve as a ligand or be converted into a substrate for TNLs linked to either $NAD^+$ or 2′,3′-cAMP, a noncanonical cyclic nucleotide monophosphate (cNMP).[50–52] Plant TIR domains of NLRs are enzymes capable of degrading $NAD^+$. While the NADase function of the TIR domain is necessary, it is not sufficient on its own to trigger

(C) Abundance of *S. indica* in Arabidopsis seedlings 14 days after germination. Fungal (*SiTEF*) to plant (*AtUbi*) ratios were calculated using cDNA as template and method $2^{-\Delta CT}$. Boxplots represent 6 independent biological replicates. Asterisks indicate a significant difference from Col-0 WT samples (Student's t test, $^{**}p < 0.01$).

(D) Root length of Arabidopsis seedlings 14 and 21 days after germination in the presence of *S. indica* or mock treatment. Boxplots show data from 23–86 biological replicates. Different letters indicate significant differences in samples from one time point using two-way ANOVA with post-hoc Tukey HSD test ($p < 0.05$). The experiment was repeated 2 times independently with similar results.

(E) Current model illustrating cell death pathways occurring during colonization of *S. indica* in Arabidopsis Col-0 (blue), *ent3* mutant (yellow), and *isi* mutant (red).

(F) The heatmap shows the expression values of *A. thaliana* NLR genes with NB-ARC and LRR (NL) domains in *A. thaliana* root samples as $\log_2$ transformed TPM values. Samples were taken at 1-, 3-, 6-, and 10-day post inoculation with *S. indica* or mock treatment. A more detailed version of the heatmap including an in-depth description can be found in Figure S13. More details about the experimental conditions underlying the dataset can also be found in Eichfeld et al.[40]

plant immune responses in Arabidopsis. Recently, it was shown that plant TIR proteins can also function as 2′,3′-cAMP/cGMP synthetases by hydrolyzing RNA/DNA. Mutations that specifically disrupt synthetase activity prevent TIR-mediated cell death in *N. benthamiana*, demonstrating an important role for these cNMPs in TIR signaling.[50] The accumulation of extracellular 3′,5′-cAMP upon *S. indica* colonization and treatment with dAdo establishes a link to cNMPs. Further research is necessary to elucidate the metabolism of dAdo in plant cells and to understand how intracellular dAdo activates TNLs in Arabidopsis. Given that TIR-domain cell-surface receptors (TLRs) and various TIR-adaptor proteins are involved in mammalian immunity, our findings suggest the potential to explore the role of TIR domains in dAdo-triggered cell death in plants and beyond. However, more biochemical evidence is needed to definitively clarify the mechanisms by which dAdo affects TNL signaling in plants.

In animal systems, it has been shown that following import of dAdo into macrophages, dAdo-mediated toxicity involves conversion of dAdo to dAMP by deoxycytidine kinase (DCK) and adenosine kinase (ADK) activity and signaling via subsequent conversion to the corresponding di- and tri-phosphates by nucleotide kinases and activation of caspase-3-induced apoptosis.[25] The absence of caspases in plants and the potential involvement of a TIR-NLR protein in dAdo-mediated cell death in Arabidopsis strongly suggest that this part of the signaling pathway is not conserved between plants and animals and relies on different regulatory and execution mechanisms that require further investigation. The role of the EDS1 family of immunity regulators, which are genetically required for pathogen resistance and execution of cell death by various TIR-NLRs,[53] in ISI-mediated cell death also remains to be explored. The potential involvement of other ISI-like proteins as interaction partners warrants further investigation, particularly given that the dAdo-resistance phenotype associated with ISI is only partial.

In summary, we have uncovered a cellular signaling pathway that responds to extracellularly produced metabolites during fungal colonization and links nucleoside transport by an ENT to cellular activation of the MEP pathway and cell death potentially influenced by the activation of ISI, a fungal-induced TIR-NLR. The observation that dAdo triggers cell death across multiple plant species, including a basal lineage, suggests that this pathway is likely conserved and represents an ancient cell death mechanism co-opted to facilitate plant-endophyte symbiosis. This paves the way for a better understanding of immunometabolism in plant-microbe interactions.

## RESOURCE AVAILABILITY

### Lead contact

Further information and requests for resources and reagents should be directed to and will be fulfilled by the lead contact, Prof. Alga Zuccaro (azuccaro@uni-koeln.de).

### Materials availability

This study did not generate new unique reagents. Plasmids and transgenic plant seeds generated in this study are available from the lead contact with a completed Materials Transfer Agreement.

### Data and code availability

- RNA-seq data generated in this study have been deposited in the Gene Expression Omnibus (GEO) database under the accession numbers GEO:GSE209761 and GEO:GSM6394981. The data are available as of the date of publication. Microscopy data reported in this paper will be shared by the lead contact upon request.
- This paper does not report original code.
- Any additional information required to reanalyze the data reported in this paper is available from the lead contact upon request.

## ACKNOWLEDGMENTS

We would like to thank Prof. Jijie Chai and Jane Parker for discussions and reading the manuscript prior to submission. We further want to thank Johana Misas Stadtel for her support during ABPP assays. N.D. was supported by the International Max Planck Research School (IMPRS) at the University of Cologne. A.Z. and M.D.Z. gratefully acknowledge support from the Cluster of Excellence on Plant Sciences (CEPLAS) funded by the German Research Foundation (DFG) under the Excellence Strategy—EXC 2048/1—project ID: 390686111. A.Z. and N.D. additionally acknowledge support from SFB 1403 project ID: 1403-414786233. We further would like to thank the US Department of Energy Joint Genome Institute (https://ror.org/04xm1d337) and Yu Zhang, Sravanthi Tejomurthula, Daniel Peterson, Vivian Ng, and Igor Grigoriev for producing sequencing data within the work proposal 10.46936/10.25585/60001292. C.-P.W. gratefully acknowledges support from DFG grant WI3411/8-1. M.D.Z. and J.S. acknowledge support from NEXTplant (IRTG 2466). Some of the graphical representations were generated using the online tool BioRender.

## AUTHOR CONTRIBUTIONS

A.Z. and N.D. designed the experiment. N.D. did characterize the role of *ENT3* and *AtISI* experimentally. H.W. did analyze the role of *Si*NucA. G.U.B. and A.T. did produce metabolomics data. H.S. and C.-P.W. did perform enzymatic assays and measured nucleotide concentrations. G.L. and C.D.Q. did perform all bioinformatic analyses. N.M.C. and S.W. did perform microscopy. P.S. did perform calcium influx and ROS burst assays. J.S. and M.D.Z. did perform protoplast assays. H.R. did support the conceptualization of the experiment and perform initial cell death assays. M.K. and A.D. did perform experiments with *Marchantia polymorpha*. The manuscript was written by A.Z. and N.D. with continuous input from all authors.

## DECLARATION OF INTERESTS

The authors declare no competing interests.

## STAR★METHODS

Detailed methods are provided in the online version of this paper and include the following:

- KEY RESOURCES TABLE
- EXPERIMENTAL MODEL AND STUDY PARTICIPANT DETAILS
  - Plant Material and Growth Conditions
  - Fungal strains and cultivation techniques
- METHOD DETAILS
  - Fungal inoculation
  - Confocal microscopy
  - DNA and RNA extraction
  - Quantitative RT-PCR analysis
  - *Serendipita indica* transformation
  - Nuclease activity test
  - *Si*NucA-HA-His purification
  - Measurement of enzyme kinetics of *Si*E5NT
  - Measurement of release of deoxynucleosides
  - PAM fluorometric measurements
  - Cell death staining with Evans blue

- Activity-based protein profiling
- RNAseq
- Collection of extracellular fluid
- Metabolite analysis
- $Ca^{2+}$ influx quantification
- Heterologous protein production in *Nicotiana benthamiana* and protein purification
- Ion leakage measurements
- Seed germination test
- Root length measurements
- Oxidative burst assay
- Protoplast isolation and transformation

- QUANTIFICATION AND STATISTICAL ANALYSIS

## SUPPLEMENTAL INFORMATION

Supplemental information can be found online at https://doi.org/10.1016/j.chom.2024.10.020.

Received: March 17, 2022
Revised: August 9, 2024
Accepted: October 31, 2024
Published: November 26, 2024

## REFERENCES

1. D'Haeze, W., De Rycke, R., Mathis, R., Goormachtig, S., Pagnotta, S., Verplancke, C., Capoen, W., and Holsters, M. (2003). Reactive oxygen species and ethylene play a positive role in lateral root base nodulation of a semiaquatic legume. Proc. Natl. Acad. Sci. USA *100*, 11789–11794. https://doi.org/10.1073/pnas.1333899100.
2. Ragnelli, A.M., Aimola, P., Maione, M., Zarivi, O., Leonardi, M., and Pacioni, G. (2014). The cell death phenomenon during Tuber ectomycorrhiza morphogenesis. Plant Biosyst. An Int. J. Dealing Aspects Plant Biol. *148*, 473–482. https://doi.org/10.1080/11263504.2013.788575.
3. Mucha, J., Guzicka, M., Ratajczak, E., and Zadworny, M. (2014). Strategies utilized by trophically diverse fungal species for Pinus sylvestris root colonization. Tree Physiol. *34*, 73–86. https://doi.org/10.1093/treephys/tpt111.
4. Deshmukh, S., Hückelhoven, R., Schäfer, P., Imani, J., Sharma, M., Weiss, M., Waller, F., and Kogel, K.H. (2006). The root endophytic fungus Piriformospora indica requires host cell death for proliferation during mutualistic symbiosis with barley. Proc. Natl. Acad. Sci. USA *103*, 18450–18457. https://doi.org/10.1073/pnas.0605697103.
5. Qiang, X., Zechmann, B., Reitz, M.U., Kogel, K.H., and Schäfer, P. (2012). The mutualistic fungus Piriformospora indica colonizes Arabidopsis roots by inducing an endoplasmic reticulum stress-triggered caspase-dependent cell death. Plant Cell *24*, 794–809. https://doi.org/10.1105/tpc.111.093260.
6. Lahrmann, U., Ding, Y., Banhara, A., Rath, M., Hajirezaei, M.R., Döhlemann, S., von Wirén, N., Parniske, M., and Zuccaro, A. (2013). Host-related metabolic cues affect colonization strategies of a root endophyte. Proc. Natl. Acad. Sci. USA *110*, 13965–13970. https://doi.org/10.1073/pnas.1301653110.
7. Oberwinkler, F., Riess, K., Bauer, R., Selosse, M.-A., Weiß, M., Garnica, S., and Zuccaro, A. (2013). Enigmatic Sebacinales. Mycol. Progress *12*, 1–27. https://doi.org/10.1007/s11557-012-0880-4.
8. Tedersoo, L., Bahram, M., Ryberg, M., Otsing, E., Kõljalg, U., and Abarenkov, K. (2014). Global biogeography of the ectomycorrhizal /sebacina lineage (Fungi, Sebacinales) as revealed from comparative phylogenetics analyses. Mol. Ecol. *23*, 4168–4183. https://doi.org/10.1111/mec.12849.
9. Weiß, M., Waller, F., Zuccaro, A., and Selosse, M.A. (2016). Sebacinales - one thousand and one interactions with land plants. New Phytol. *211*, 20–40. https://doi.org/10.1111/nph.13977.
10. Zuccaro, A., Lahrmann, U., Güldener, U., Langen, G., Pfiffi, S., Biedenkopf, D., Wong, P., Samans, B., Grimm, C., Basiewicz, M., et al. (2011). Endophytic Life Strategies Decoded by Genome and Transcriptome Analyses of the Mutualistic Root Symbiont Piriformospora indica. Plos Pathog. *7*, e1002290. https://doi.org/10.1371/journal.ppat.1002290.
11. Lahrmann, U., and Zuccaro, A. (2012). Opprimo ergo sum-Evasion and Suppression in the Root Endophytic Fungus Piriformospora indica. Mol. Plant Microbe Interact. *25*, 727–737. https://doi.org/10.1094/MPMI-11-11-0291.
12. Lahrmann, U., Strehmel, N., Langen, G., Frerigmann, H., Leson, L., Ding, Y., Scheel, D., Herklotz, S., Hilbert, M., and Zuccaro, A. (2015). Mutualistic root endophytism is not associated with the reduction of saprotrophic traits and requires a noncompromised plant innate immunity. New Phytol. *207*, 841–857. https://doi.org/10.1111/nph.13411.
13. Nizam, S., Qiang, X., Wawra, S., Nostadt, R., Getzke, F., Schwanke, F., Dreyer, I., Langen, G., and Zuccaro, A. (2019). Serendipita indica E5'NT modulates extracellular nucleotide levels in the plant apoplast and affects fungal colonization. EMBO Rep. *20*, e47430. https://doi.org/10.15252/embr.201847430.
14. Schneider, H.M., and Lynch, J.P. (2018). Functional implications of root cortical senescence for soil resource capture. Plant Soil *423*, 13–26. https://doi.org/10.1007/s11104-017-3533-1.
15. Presti, L., Lanver, D., Schweizer, G., Tanaka, S., Liang, L., Tollot, M., Zuccaro, A., Reissmann, S., Kahmann, R., and Merchant, S. (2015). Fungal effectors and plant susceptibility. Annu. Rev. Plant Biol. *66*, 513–545. https://doi.org/10.1146/annurev-arplant-043014-114623.
16. Kloppholz, S., Kuhn, H., and Requena, N. (2011). A Secreted Fungal Effector of Glomus intraradices Promotes Symbiotic Biotrophy. Curr. Biol. *21*, 1204–1209. https://doi.org/10.1016/j.cub.2011.06.044.
17. Plett, J.M., Daguerre, Y., Wittulsky, S., Vayssières, A., Deveau, A., Melton, S.J., Kohler, A., Morrell-Falvey, J.L., Brun, A., Veneault-Fourrey, C., and Martin, F. (2014). Effector MiSSP7 of the mutualistic fungus Laccaria bicolor stabilizes the Populus JAZ6 protein and represses jasmonic acid (JA) responsive genes. Proc. Natl. Acad. Sci. USA *111*, 8299–8304. https://doi.org/10.1073/pnas.1322671111.
18. Wawra, S., Fesel, P., Widmer, H., Timm, M., Seibel, J., Leson, L., Kesseler, L., Nostadt, R., Hilbert, M., Langen, G., and Zuccaro, A. (2016). The fungal-specific beta-glucan-binding lectin FGB1 alters cell-wall composition and suppresses glucan-triggered immunity in plants. Nat. Commun. *7*, 13188. https://doi.org/10.1038/ncomms13188.
19. Voß, S., Betz, R., Heidt, S., Corradi, N., and Requena, N. (2018). RiCRN1, a Crinkler Effector From the Arbuscular Mycorrhizal Fungus Rhizophagus irregularis, Functions in Arbuscule Development. Front. Microbiol. *9*, 2068. https://doi.org/10.3389/fmicb.2018.02068.
20. Nostadt, R., Hilbert, M., Nizam, S., Rovenich, H., Wawra, S., Martin, J., Küpper, H., Mijovilovich, A., Ursinus, A., Langen, G., et al. (2020). A secreted fungal histidine- and alanine-rich protein regulates metal ion homeostasis and oxidative stress. New Phytol. *227*, 1174–1188. https://doi.org/10.1111/nph.16606.
21. Antonioli, L., Pacher, P., Vizi, E.S., and Haskó, G. (2013). CD39 and CD73 in immunity and inflammation. Trends Mol. Med. *19*, 355–367. https://doi.org/10.1016/j.molmed.2013.03.005.
22. Pham, A.Q., Cho, S.-H., Nguyen, C.T., and Stacey, G. (2020). Arabidopsis Lectin Receptor Kinase P2K2 Is a Second Plant Receptor for Extracellular ATP and Contributes to Innate Immunity1 [OPEN]. Plant Physiol. *183*, 1364–1375. https://doi.org/10.1104/pp.19.01265.
23. Thürich, J., Meichsner, D., Furch, A.C.U., Pfalz, J., Krüger, T., Kniemeyer, O., Brakhage, A., and Oelmüller, R. (2018). Arabidopsis thaliana responds to colonisation of Piriformospora indica by secretion of symbiosis-specific proteins. PLoS ONE *13*, e0209658. https://doi.org/10.1371/journal.pone.0209658.
24. Thammavongsa, V., Missiakas, D.M., and Schneewind, O. (2013). Staphylococcus aureus degrades neutrophil extracellular traps to promote immune cell death. Science *342*, 863–866. https://doi.org/10.1126/science.1242255.

25. Winstel, V., Missiakas, D., and Schneewind, O. (2018). Staphylococcus aureus targets the purine salvage pathway to kill phagocytes. Proc. Natl. Acad. Sci. USA *115*, 6846–6851. https://doi.org/10.1073/pnas.1805622115.

26. Rafiqi, M., Jelonek, L., Akum, N.F., Zhang, F., and Kogel, K.H. (2013). Effector candidates in the secretome of Piriformospora indica, a ubiquitous plant-associated fungus. Front. Plant Sci. *4*, 228. https://doi.org/10.3389/fpls.2013.00228.

27. Kolodziejek, I., Misas-Villamil, J.C., Kaschani, F., Clerc, J., Gu, C., Krahn, D., Niessen, S., Verdoes, M., Willems, L.I., Overkleeft, H.S., et al. (2011). Proteasome Activity Imaging and Profiling Characterizes Bacterial Effector Syringolin A. Plant Physiol. *155*, 477–489. https://doi.org/10.1104/pp.110.163733.

28. Olvera-Carrillo, Y., Van Bel, M., Van Hautegem, T., Fendrych, M., Huysmans, M., Simaskova, M., van Durme, M., Buscaill, P., Rivas, S., Coll, N.S., et al. (2015). A Conserved Core of Programmed Cell Death Indicator Genes Discriminates Developmentally and Environmentally Induced Programmed Cell Death in Plants. Plant Physiol. *169*, 2684–2699. https://doi.org/10.1104/pp.15.00769.

29. Xiao, Y., Savchenko, T., Baidoo, E.E.K., Chehab, W.E., Hayden, D.M., Tolstikov, V., Corwin, J.A., Kliebenstein, D.J., Keasling, J.D., and Dehesh, K. (2012). Retrograde signaling by the plastidial metabolite MEcPP regulates expression of nuclear stress-response genes. Cell *149*, 1525–1535. https://doi.org/10.1016/j.cell.2012.04.038.

30. Zipfel, C., and Oldroyd, G.E.D. (2017). Plant signalling in symbiosis and immunity. Nature *543*, 328–336. https://doi.org/10.1038/nature22009.

31. Ngou, B.P.M., Ahn, H.K., Ding, P., and Jones, J.D.G. (2021). Mutual potentiation of plant immunity by cell-surface and intracellular receptors. Nature *592*, 110–115. https://doi.org/10.1038/s41586-021-03315-7.

32. Yuan, M., Jiang, Z., Bi, G., Nomura, K., Liu, M., Wang, Y., Cai, B., Zhou, J.M., He, S.Y., and Xin, X.F. (2021). Pattern-recognition receptors are required for NLR-mediated plant immunity. Nature *592*, 105–109. https://doi.org/10.1038/s41586-021-03316-6.

33. Choi, J., Tanaka, K., Cao, Y., Qi, Y., Qiu, J., Liang, Y., Lee, S.Y., and Stacey, G. (2014). Identification of a plant receptor for extracellular ATP. Science *343*, 290–294. https://doi.org/10.1126/science.343.6168.290.

34. Tanaka, K., Choi, J., Cao, Y., and Stacey, G. (2014). Extracellular ATP acts as a damage-associated molecular pattern (DAMP) signal in plants. Front. Plant Sci. *5*, 446. https://doi.org/10.3389/fpls.2014.00446.

35. Kilian, J., Whitehead, D., Horak, J., Wanke, D., Weinl, S., Batistic, O., D'Angelo, C., Bornberg-Bauer, E., Kudla, J., and Harter, K. (2007). The AtGenExpress global stress expression data set: protocols, evaluation and model data analysis of UV-B light, drought and cold stress responses. Plant J. *50*, 347–363. https://doi.org/10.1111/j.1365-313X.2007.03052.x.

36. Li, G., Liu, K., Baldwin, S.A., and Wang, D. (2003). Equilibrative nucleoside transporters of Arabidopsis thaliana. cDNA cloning, expression pattern, and analysis of transport activities. J. Biol. Chem. *278*, 35732–35742. https://doi.org/10.1074/jbc.M304768200.

37. Rich-Griffin, C., Stechemesser, A., Finch, J., Lucas, E., Ott, S., and Schäfer, P. (2020). Single-Cell Transcriptomics: A High-Resolution Avenue for Plant Functional Genomics. Trends Plant Sci. *25*, 186–197. https://doi.org/10.1016/j.tplants.2019.10.008.

38. Ordon, J., Kiel, N., Becker, D., Kretschmer, C., Schulze-Lefert, P., and Stuttmann, J. (2023). Targeted gene deletion with SpCas9 and multiple guide RNAs in Arabidopsis thaliana: four are better than two. Plant Methods *19*, 30. https://doi.org/10.1186/s13007-023-01010-4.

39. Stuttmann, J., Barthel, K., Martin, P., Ordon, J., Erickson, J.L., Herr, R., Ferik, F., Kretschmer, C., Berner, T., Keilwagen, J., et al. (2021). Highly efficient multiplex editing: one-shot generation of 8x Nicotiana benthamiana and 12x Arabidopsis mutants. Plant J. *106*, 8–22. https://doi.org/10.1111/tpj.15197.

40. Eichfeld, R., Mahdi, L.K., De Quattro, C., Armbruster, L., Endeshaw, A.B., Miyauchi, S., Hellmann, M.J., Cord-Landwehr, S., Peterson, D., Singan, V., et al. (2024). Transcriptomics reveal a mechanism of niche defense: two beneficial root endophytes deploy an antimicrobial GH18-CBM5 chitinase to protect their hosts. New Phytol. *244*, 980–996. https://doi.org/10.1111/nph.20080.

41. Thammavongsa, V., Kern, J.W., Missiakas, D.M., and Schneewind, O. (2009). Staphylococcus aureus synthesizes adenosine to escape host immune responses. J. Exp. Med. *206*, 2417–2427. https://doi.org/10.1084/jem.20090097.

42. Brinkmann, V., Reichard, U., Goosmann, C., Fauler, B., Uhlemann, Y., Weiss, D.S., Weinrauch, Y., and Zychlinsky, A. (2004). Neutrophil extracellular traps kill bacteria. Science *303*, 1532–1535. https://doi.org/10.1126/science.1092385.

43. Driouich, A., Smith, C., Ropitaux, M., Chambard, M., Boulogne, I., Bernard, S., Follet-Gueye, M.L., Vicré, M., and Moore, J. (2019). Root extracellular traps versus neutrophil extracellular traps in host defence, a case of functional convergence? Biol. Rev. Camb. Philos. Soc. *94*, 1685–1700. https://doi.org/10.1111/brv.12522.

44. Chambard, M., Plasson, C., Derambure, C., Coutant, S., Tournier, I., Lefranc, B., Leprince, J.M., Kiefer-Meyer, M.C., Driouich, A., Follet-Gueye, M.L., and Boulogne, I. (2021). New Insights into Plant Extracellular DNA. A Study in Soybean Root Extracellular Trap. Cells *10*, ARTN69. https://doi.org/10.3390/cells10010069.

45. Tran, T.M., MacIntyre, A., Hawes, M., and Allen, C. (2016). Escaping Underground Nets: Extracellular DNases Degrade Plant Extracellular Traps and Contribute to Virulence of the Plant Pathogenic Bacterium Ralstonia solanacearum. PLoS Pathog. *12*, e1005686. https://doi.org/10.1371/journal.ppat.1005686.

46. Hawes, M., Allen, C., Turgeon, B.G., Curlango-Rivera, G., Minh Tran, T.M., Huskey, D.A., and Xiong, Z.G. (2016). Root Border Cells and Their Role in Plant Defense. Annu. Rev. Phytopathol. *54*, 143–161. https://doi.org/10.1146/annurev-phyto-080615-100140.

47. Wu, Z., Li, M., Dong, O.X., Xia, S., Liang, W., Bao, Y., Wasteneys, G., and Li, X. (2019). Differential regulation of TNL-mediated immune signaling by redundant helper CNLs. New Phytol. *222*, 938–953. https://doi.org/10.1111/nph.15665.

48. Saur, I.M.L., Panstruga, R., and Schulze-Lefert, P. (2021). NOD-like receptor-mediated plant immunity: from structure to cell death. Nat. Rev. Immunol. *21*, 305–318. https://doi.org/10.1038/s41577-020-00473-z.

49. Kim, T.H., Kunz, H.H., Bhattacharjee, S., Hauser, F., Park, J., Engineer, C., Liu, A., Ha, T., Parker, J.E., Gassmann, W., and Schroeder, J.I. (2012). Natural variation in small molecule-induced TIR-NB-LRR signaling induces root growth arrest via EDS1- and PAD4-complexed R protein VICTR in Arabidopsis. Plant Cell *24*, 5177–5192. https://doi.org/10.1105/tpc.112.107235.

50. Yu, D., Song, W., Tan, E.Y.J., Liu, L., Cao, Y., Jirschitzka, J., Li, E., Logemann, E., Xu, C., Huang, S., et al. (2022). TIR domains of plant immune receptors are 2',3'-cAMP/cGMP synthetases mediating cell death. Cell *185*, 2370–2386.e18. https://doi.org/10.1016/j.cell.2022.04.032.

51. Wan, L., Essuman, K., Anderson, R.G., Sasaki, Y., Monteiro, F., Chung, E.H., Osborne Nishimura, E., DiAntonio, A., Milbrandt, J., Dangl, J.L., and Nishimura, M.T. (2019). TIR domains of plant immune receptors are NAD(+)-cleaving enzymes that promote cell death. Science *365*, 799–803. https://doi.org/10.1126/science.aax1771.

52. Horsefield, S., Burdett, H., Zhang, X., Manik, M.K., Shi, Y., Chen, J., Qi, T., Gilley, J., Lai, J.S., Rank, M.X., et al. (2019). NAD(+) cleavage activity by animal and plant TIR domains in cell death pathways. Science *365*, 793–799. https://doi.org/10.1126/science.aax1911.

53. Lapin, D., Bhandari, D.D., and Parker, J.E. (2020). Origins and Immunity Networking Functions of EDS1 Family Proteins. Annu. Rev. Phytopathol. *58*, 253–276. https://doi.org/10.1146/annurev-phyto-010820-012840.

54. Wawra, S., Fesel, P., Widmer, H., Neumann, U., Lahrmann, U., Becker, S., Hehemann, J.H., Langen, G., and Zuccaro, A. (2019). FGB1 and WSC3 are in planta-induced beta-glucan-binding fungal lectins with different functions. New Phytol. *222*, 1493–1506. https://doi.org/10.1111/nph.15711.

55. Marquès-Bueno, M.D.M., Morao, A.K., Cayrel, A., Platre, M.P., Barberon, M., Caillieux, E., Colot, V., Jaillais, Y., Roudier, F., and Vert, G. (2016). A versatile Multisite Gateway-compatible promoter and transgenic line

collection for cell type-specific functional genomics in Arabidopsis. Plant J. *85*, 320–333. https://doi.org/10.1111/tpj.13099.

56. Schindelin, J., Arganda-Carreras, I., Frise, E., Kaynig, V., Longair, M., Pietzsch, T., Preibisch, S., Rueden, C., Saalfeld, S., Schmid, B., et al. (2012). Fiji: an open-source platform for biological-image analysis. Nat. Methods *9*, 676–682. https://doi.org/10.1038/nmeth.2019.
57. Bolger, A.M., Lohse, M., and Usadel, B. (2014). Trimmomatic: a flexible trimmer for Illumina sequence data. Bioinformatics *30*, 2114–2120. https://doi.org/10.1093/bioinformatics/btu170.
58. Bray, N.L., Pimentel, H., Melsted, P., and Pachter, L. (2016). Near-optimal probabilistic RNA-seq quantification. Nat. Biotechnol. *34*, 525–527. https://doi.org/10.1038/nbt.3519.
59. Soneson, C., Love, M.I., and Robinson, M.D. (2015). Differential analyses for RNA-seq: transcript-level estimates improve gene-level inferences. F1000Res *4*, 1521. https://doi.org/10.12688/f1000research.7563.2.
60. Love, M.I., Huber, W., and Anders, S. (2014). Moderated estimation of fold change and dispersion for RNA-seq data with DESeq2. Genome Biol. *15*, 550. https://doi.org/10.1186/s13059-014-0550-8.
61. Hilbert, M., Voll, L.M., Ding, Y., Hofmann, J., Sharma, M., and Zuccaro, A. (2012). Indole derivative production by the root endophyte Piriformospora indica is not required for growth promotion but for biotrophic colonization of barley roots. New Phytol. *196*, 520–534. https://doi.org/10.1111/j.1469-8137.2012.04275.x.
62. Livak, K.J., and Schmittgen, T.D. (2001). Analysis of Relative Gene Expression Data Using Real-Time Quantitative PCR and the $2^{-\Delta\Delta CT}$ Method. Methods *25*, 402–408. https://doi.org/10.1006/meth.2001.1262.
63. Werner, A.K., Sparkes, I.A., Romeis, T., and Witte, C.P. (2008). Identification, biochemical characterization, and subcellular localization of allantoate amidohydrolases from Arabidopsis and soybean. Plant Physiol. *146*, 418–430. https://doi.org/10.1104/pp.107.110809.
64. Myrach, T., Zhu, A., and Witte, C.P. (2017). The assembly of the plant urease activation complex and the essential role of the urease accessory protein G (UreG) in delivery of nickel to urease. J. Biol. Chem. *292*, 14556–14565. https://doi.org/10.1074/jbc.M117.780403.
65. Straube, H., Niehaus, M., Zwittian, S., Witte, C.P., and Herde, M. (2021). Enhanced nucleotide analysis enables the quantification of deoxynucleotides in plants and algae revealing connections between nucleoside and deoxynucleoside metabolism. Plant Cell *33*, 270–289. https://doi.org/10.1093/plcell/koaa028.
66. Vijayaraghavareddy, P., Adhinarayanreddy, V., Vemanna, R.S., Sreeman, S., and Makarla, U. (2017). Quantification of Membrane Damage/Cell Death Using Evan's Blue Staining Technique. Bio Protoc. *7*, e2519. https://doi.org/10.21769/BioProtoc.2519.
67. Wanke, A., Rovenich, H., Schwanke, F., Velte, S., Becker, S., Hehemann, J.H., Wawra, S., and Zuccaro, A. (2020). Plant species-specific recognition of long and short beta-1,3-linked glucans is mediated by different receptor systems. Plant J. *102*, 1142–1156. https://doi.org/10.1111/tpj.14688.
68. Ochoa-Fernandez, R., Abel, N.B., Wieland, F.G., Schlegel, J., Koch, L.A., Miller, J.B., Engesser, R., Giuriani, G., Brandl, S.M., Timmer, J., et al. (2020). Optogenetic control of gene expression in plants in the presence of ambient white light. Nat. Methods *17*, 717–725. https://doi.org/10.1038/s41592-020-0868-y.

## STAR★METHODS

### KEY RESOURCES TABLE

| REAGENT or RESOURCE | SOURCE | IDENTIFIER |
|---|---|---|
| **Antibodies** | | |
| Mouse Monoclonal Anti-HA | Sigma-Aldrich | RRID:AB_260092 |
| Conjugated Monoclonal Anti-StrepII + HRP | Iba life sciences | RRID:AB_3095590 |
| **Bacterial and virus strains** | | |
| *Escherichia coli* Mach1 | Lab strain | N/A |
| *Agrobacterium tumefaciens* GV3101 pmp90RK | Lab strain | N/A |
| *Serendipita indica* | German Collection of Microorganisms and Cell Cultures | DSM11827 |
| **Biological samples** | | |
| *Arabidopsis thaliana* Col-0 | NASC | N60000 |
| *Hordeum vulgare* "Golden Promise" | Lab stock | N/A |
| *Nicotiana benthamiana* | Lab stock | N/A |
| *Marchantia polymorpha* Tak1 | Lab stock | N/A |
| *Marchantia polymorpha* Tak2 | Lab stock | N/A |
| **Chemicals, peptides, and recombinant proteins** | | |
| WGA-AF488 (Oregon Green) | Invitrogen /ThermoFisher | Catalogue No: W6748 |
| DAPI | Invitrogen /ThermoFisher | Catalogue No: D1306 |
| FGB1-FITC488 | Wawra et al.[54] | N/A |
| SYTOX Orange | Invitrogen /ThermoFisher | Catalogue No: S11368 |
| dAdo | Sigma-Aldrich | CAS No: 16373-93-6 |
| Evans blue | Sigma-Aldrich | CAS No: 314-13-6 |
| Adenosine | Sigma-Aldrich | CAS No: 58-61-7 |
| SyproRuby | Invitrogen /ThermoFisher | Catalogue No: S12000 |
| Coomassie Brilliant Blue | RAL Diagnostics | 362740-0025 |
| MVB072 | Kolodziejek et al.[27] | N/A |
| Flg22 | GenScript | Cat. No: RP19986 |
| AMP | Sigma-Aldrich | CAS No: 4578-31-8 |
| dAMP | Sigma-Aldrich | CAS No: 653-63-4 |
| ADP | Sigma-Aldrich | CAS No: 20398-34-9 |
| dADP | Sigma-Aldrich | CAS No: 72003-83-9 |
| ATP | Sigma-Aldrich | CAS No: 34369-07-8 |
| dATP | Sigma-Aldrich | CAS No: 74299-50-6 |
| Coelenterazine | Roth | CAS No: 55779-48-1 |
| Horseradish Peroxidase | Sigma-Aldrich | CAS No: 9003-99-0 |
| Cellulase "Onozuka R-10" | SERVA Electrophoresis GmbH | CAS No: 9012-54-8 |
| Macerozyme R10 | SERVA Electrophoresis GmbH | CAS No: 9032-75-1 |
| D-Luciferin | Biosynth | CAS No: 115144-35-9 |
| FM4-64 | Invitrogen /ThermoFisher | Catalogue No: F34653 |
| **Critical commercial assays** | | |
| First strand cDNA synthesis kit | ThermoFisher | Catalogue No: K1612 |
| GoTaq® qPCR Master Mix, 2X | Promega | Catalogue No: A600A |
| NucleoSpin Plasmid prep | Macherey & Nagel | Catalogue No: 740588 |
| NucleoSpin Gel & PCR Clean-Up | Macherey & Nagel | Catalogue No: 740609 |
| Gateway BP clonase II Enzyme mix | Invitrogen/ThermoFisher | Catalogue No: 11789020 |
| Gateway LR clonase II Enzyme mix | Invitrogen/ThermoFisher | Catalogue No: 11791020 |

(*Continued on next page*)

*Continued*

| REAGENT or RESOURCE | SOURCE | IDENTIFIER |
|---|---|---|
| **Deposited data** | | |
| RNASeq data: Arabidopsis after dAdo treatment | this paper | GEO database: GSE209761 & GSM6394981 |
| **Experimental models: Organisms/strains** | | |
| *Arabidopsis: UBQ10:H2B:mCherry* | Marquès-Bueno et al.[55] | N/A |
| *Arabidopsis: 35S:SiNucA* | this paper | N/A |
| *Arabidopsis: 35S:SiNucA:mCherry* | this paper | N/A |
| *Arabidopsis: 35S:SiNucA:mCherry(w/o SP)* | this paper | N/A |
| *Arabidopsis: Col-0$^{AEQ}$* | Choi et al.[33] | N/A |
| *Arabidopsis: Col-0$^{AEQ}$ Δdorn1* | Choi et al.[33] | N/A |
| *Arabidopsis: ent3* | NASC | SALK_204257C |
| *Arabidopsis: ent1* | NASC | SALK_025174C |
| *Arabidopsis: isi* | NASC | SALK_034517C |
| *Arabidopsis: CRISPRisi* | this paper | N/A |
| *Serendipita indica: FGB1:SiNucA:HA:His* | this paper | N/A |
| **Oligonucleotides** | | |
| All oligonucleotides are listed in Table S8. | N/A | N/A |
| **Recombinant DNA** | | |
| *FGB1:SiNucA:HA:His* for stable fungal transformation | this paper | N/A |
| *35S:SiNucA* for stable Arabidopsis transformation | this paper | N/A |
| *35S:SiNucA:mCherry* for stable Arabidopsis transformation | this paper | N/A |
| *35S:SiNucA:mCherry (w/o SP)* for stable Arabidopsis transformation | this paper | N/A |
| *pDGE347_Cas9_4xsgRNA)* for stable Arabidopsis transformation targeting ISI for CRISPR-CAS9-induced KO | this paper | N/A |
| **Software and algorithms** | | |
| Prism 8 | Graphpad | https://www.graphpad.com/ |
| Fiji software | Schindelin et al.[56] | https://imagej.net/software/fiji/ |
| Trimmomatic v.0.36 | Bolger et al.[57] | https://github.com/usadellab/Trimmomatic |
| Kallisto v.0.46.2 | Bray et al.[58] | https://github.com/pachterlab/kallisto |
| R package: tximport | Soneson et al.[59] | https://github.com/thelovelab/tximport |
| R package: DESeq2 | Love et al.[60] | https://github.com/thelovelab/DESeq2 |

## EXPERIMENTAL MODEL AND STUDY PARTICIPANT DETAILS

### Plant Material and Growth Conditions

Seeds of *A. thaliana* ecotype Columbia 0 (Col-0), Col-0$^{AEQ}$, and Col-0$^{AEQ}$ *dorn1*,[33] the SALK lines SALK_034517C (*isi*), SALK_204257C (*ent3*) and SALK_025174C were used in the experiments. SALK lines and a matching Col-0 control were obtained from the Nottingham Arabidopsis Stock Centre (NASC, http://arabidopsis.info/).

In addition, Col-0 expressing histone H2B fused to mCherry (H2B:2xmCherry) under the UBQ10 promoter in root cells[55] were used in this study. Col-0 transformation was performed using the floral dip method as described in Nizamet al.[13] to generate the transgenic lines *35S::SiNucA*, *35S::SiNucA:mCherry* (with and without signal peptide) and the *CRISPRisi* line.

Arabidopsis seeds were surface sterilized (70 % ethanol for 10 minutes, 100 % ethanol for 7 minutes) and after 3 days of stratification, grown on ½ MS medium (Murashige-Skoog medium, with vitamins, pH 5.7) containing 1% (w/v) sucrose and 0.4% (w/v) Gelrite under short-day conditions (8 h light, 16 h dark) with 130 μmol m-2 s-1 light and 22 °C/18 °C. Two methods were used for fungal inoculation: 1) 7-day-old seedlings were transferred to ½ MS without sucrose or 1/10 PNM (Plant Nutrition Medium, pH 5.7) plates (15-20 seedlings per plate). 1 ml of water containing 5x10$^5$ chlamydospores of *S. indica* was pipetted onto the root and surrounding area. Control plants were inoculated with sterile water. 2) Sterile *A. thaliana* seeds were incubated in 1 ml of water containing 5x10$^5$ *S. indica* chlamydospores for one hour and then pipetted onto 1/10 PNM plates.

For experiments using barley, seeds of the cultivar "Golden Promise" were used. The seeds were surface sterilized with 6 % sodium hypochlorite for one hour under continuous shaking and subsequently washed with sterile water for four hours, including water

exchanges every 30 minutes. The sterilized seeds were transferred to petri dishes onto autoclaved filter papers wetted with 3 ml sterile water. After four days of germination in the dark at room temperature (20 °C, high temperatures inhibit germination), the germinated seedlings were transferred onto 1/10 PNM medium in sterile mason jars.

1/10 PNM medium contains: 0.005 % (w/v) $KNO_3$, 0.005 % (w/v) $KH_2PO_4$, 0.0025 % (w/v) $K_2HPO_4$, 0.049 % (w/v) $MgSO_4$, 0.00472 % (w/v) $Ca(NO_3)_2$, 0.0025 % (w/v) NaCl, 0.5 % (v/v) Fe-EDTA stock solution and 1.2 % (w/v) Gelrite. After the pH was adjusted to 5.6, the medium was autoclaved and 1 % (v/v) 1 M MES (pH 5.6) was added.

The Fe-EDTA stock solution contains: 2.78 % (w/v) $FeSO_4$ x 7 $H_2O$ & 4.13 % (w/v) $Na_2EDTA$ x 2 $H_2O$.

Barley plants were grown at a day/night cycle of 16/8 hours, 60 % humidity and a light intensity of 108 μmol/$m_2$s.

For *Marchantia polymorpha*, the gemmae of the male Tak1 and female Tak2 gametophytes were cultured on half-strength B5 medium (1.5 g /l of 1/2 Gamborg B5 salt mixture, 0.5 g/l of MES, 10 g/l sucrose, 10 g/l plant agar – pH set to 5.2 with KOH) under continuous light.

### Fungal strains and cultivation techniques

*S. indica* strain DSM11827 (German Collection of Microorganisms and Cell Cultures, Braunschweig, Germany) was cultured on complete medium (CM) as previously described in Hilbert et al.[61]

CM medium contains: 5 % (v/v) 20 x salt solution, 2 % (w/v) glucose, 0.2 % peptone (w/v), 0.1 % (w/v) yeast extract, 0.1 % (w/v) casamine acids, 0.1 % microelement solution (v/v) & 1.5 % (w/v) agar.

The 20x salt solution contains 12 % (w/v) $NaNO_3$, 1.04 % (w/v) KCl, 1.04 % (w/v) $MgSO_4$ x 7 $H_2O$ & 3.04 % (w/v) $KH_2PO_4$. The microelement solution contains 0.6 % (w/v) $MnCl_2$ x 4 $H_2O$, 0.15 % (w/v) $H_3BO_3$, 0.265 % (w/v) $ZnSO_4$ x 7 $H_2O$, 0.075 % (w/v) KI, 0.00024 % (w/v) $Na_2MO_4$ x 2 $H_2O$ & 0.013 % (w/v) $CuSO_4$ x 5 $H_2O$.

Liquid (CM) cultures were incubated from spores at 28 °C and 120 rpm. Spores were collected from 4 weeks old plates.

## METHOD DETAILS

### Fungal inoculation

Two methods were used for fungal inoculation: 1) 7-day-old seedlings were transferred to ½ MS without sucrose or 1/10 PNM (Plant Nutrition Medium, pH 5.7) plates (15-20 seedlings per plate). 1 ml of water containing 5x$10^5$ chlamydospores of *S. indica* was pipetted onto the root and surrounding area. Control plants were inoculated with sterile water. 2) Sterile A. thaliana seeds were incubated in 1 ml of water containing 5x$10^5$ *S. indica* chlamydospores for one hour and then pipetted onto 1/10 PNM plates.

For harvesting, individual roots were thoroughly washed with water, a 4 cm root section was cut 0.5 cm below the shoot, and immediately frozen in liquid nitrogen. Two to three plates of 20 seedlings each were pooled per replicate.

### Confocal microscopy

Colonized Arabidopsis roots were treated with 5 μg/ml Wheat Germ Agglutinin-Alexa Fluor 488 conjugate (WGA-AF 488, Life Technologies, Thermo Fisher Scientific, Schwerte, Germany) or 1 μM FGB1-FITC of[54] To visualize the fungal cell wall. 250 ng/ml 4',6-diamidino-2'-phenylindole dihydrochloride (DAPI) or 500 nM SYTOX Orange (Life Technologies, Thermo Fisher Scientific, Schwerte, Germany) were used as nucleic acid stain.

A TCS SP8 confocal microscope (Leica, Wetzlar, Germany) was used for confocal laser scanning microscopy on living cells. AF 488 and FITC were excited with an argon laser at 488 nm, and the emitted light was detected with a hybrid detector at 500-550 nm. mCherry and SYTOX orange were excited with a DPSS laser at 561 nm, and the signal was detected with a hybrid detector at 590-660 nm. DAPI was excited with a diode laser at 405 nm, and the emitted light was detected with a hybrid detector at 415-460 nm.

### DNA and RNA extraction

DNA was extracted from frozen root or fungal material as described in Wawra et al.[18] Briefly, approximately 500 mg of ground frozen material was dissolved in 1 ml of CTAB extraction buffer (100 mM TrisHCl pH 7.5, 50 mM EDTA pH 8, 1.5 M NaCl, 2% (w/v) cetyltrimethylammonium bromide, 0.05% (v/v) ß-mercaptoethanol) and homogenized for 10 min. 500 μl chloroform:isoamyl alcohol mixture (24:1) was added and the tubes were mixed and centrifuged for 5 min. Ethanol and 1 volume of chloroform:isoamyl alcohol mixture (24:1) were added to the upper phase and centrifuged again. The DNA in the upper phase was precipitated with 1 volume of isopropanol at 4 °C for 1 h.

RNA was extracted with TRIzol (Invitrogen, Thermo Fisher Scientific, Schwerte, Germany) and DNA was digested with DNase I (Thermo Fisher Scientific, Schwerte, Germany) according to the manufacturer's instructions. cDNA was synthesized using the Fermentas First Strand cDNA Synthesis Kit (Thermo Fisher Scientific, Schwerte, Germany).

### Quantitative RT-PCR analysis

For quantitative real-time PCR, the 2x GoTaq qPCR Master Mix (Promega, Mannheim, Germany) was used. 500 nM forward and reverse primers and 10-20 ng of cDNA or gDNA template were added to each. The reaction was performed in a CFX connect real time system (BioRad, Munich, Germany) with the following program: 95°C 3min, 95°C 15s, 59°C 20s, 72°C 30s, 40 cycles and melting curve analysis. Relative expression was calculated using the $2^{-\Delta\Delta CT}$ method.[62] All oligonucleotides used can be found in Table S8.

### *Serendipita indica* transformation

*S. indica* protoplasts were transformed using the PEG-mediated transformation system as described in Wawra et al.[54]: For the transformation of *S. indica*, a 250 ml culture in liquid CM was inoculated with 1 ml of a spore solution set to a concentration of 2.5 x $10^4$ spores/ml and grown for 7 days at 28°C with 120 rpm of shaking. After 7 days the mycelium was collected by filtration through a Miracloth filter and washed with 50 ml 0.9 % NaCl solution before it was re-suspended in 20 ml fresh CM. The mycelial aggregates were disrupted using a Microtron® MB550 homogenizer (Kinematica, Lucerne, Switzerland) for 10 s and the homogenized culture was regenerated for 3 days at 28°C with 120 rpm of shaking in a total volume of 150 ml fresh CM. After regeneration the young mycelium was filtered again through a Miracloth filter and washed with 50 ml of 0.9 % NaCl solution to remove spores and residual medium. Protoplastation was carried out by re-suspending the filtrated mycelium in sterile filtrated 20 ml SMC buffer (1.33 M sorbitol, 50 mM $CaCl_2$ x 2H2O, 20 mM MES, pH 5.8) supplemented with 2 % (w/v) *Trichoderma harzianum* lysing enzymes (Sigma Aldrich, Taufkirchen, Germany). After incubation for 2 h at 32°C with 100 rpm of shaking the protoplastation was checked microscopically and the reaction was stopped by filtration through a Miracloth filter and addition of an equal volume of cold STC buffer (1 M sorbitol, 50 mM $CaCl_2$ x $2H_2O$, 10 mM Tris-HCl, pH 7.5). The protoplasts in the filtrate were pelleted at 3,000 xg in a swing out rotor for 10 min and washed three times with cold STC. The protoplasts were finally re-suspended in an appropriate volume of cold STC and stored on ice until transformation. 50 μg of the plasmid DNA were linearized by incubation with 20 units of the restriction enzyme *BsaAI* and precipitated for 10 min at room temperature by addition of 0.5 volumes of 7.5 M ammonium acetate and 2 volumes of 100 % isopropanol. The plasmid DNA was pelleted by centrifugation for 30 min at 17,000 x g, washed twice with 75 % ethanol, dried for 5 min at room temperature and finally re-suspended in 12 μl sterile ddH2O. For a single transformation reaction 70 μl of protoplast solution was mixed with 10 μl linearized vector, 1 μl of a 15 mg/ml heparin solution and 10 units *BsaAI* on ice and incubated for 10 min. Subsequently, 0.5 ml of a freshly prepared ice cold, filter sterilized (0.45 μm filter) STC solution supplemented with 40 % (w/v) PEG 3350 (Sigma Aldrich, Taufkirchen, Germany) was added followed by a further incubation for 15 min on ice. Finally, the protoplast solution was mixed with 5 ml of the MYP top medium (0.7 % (w/v) malt extract, 0.1 % (w/v) peptone, 0.05 % (w/v) yeast extract, 0.6 % (w/v) agar, 0.3 M sucrose) which was kept at 45°C to prevent solidification and distributed on 20 ml solidified MYP bottom medium (0.7 % (w/v) malt extract, 0.1 % (w/v) peptone, 0.05 % (w/v) yeast extract, 1.2 % (w/v) agar, 0.3 M sucrose) containing 80 μg/ml hygromycin for selection of positive transformants. After solidification of the top medium the plates were incubated at 28°C. All clones that were further used were checked whether they were homokaryotic or dikaryotic.

### Nuclease activity test

To assay the nuclease activity of the purified protein, 10 nM *Si*NucA was mixed with 100 ng linearized plasmid, 1 μg gDNA, or 1 μg RNA in buffer (5 mM Tris pH 8, 1 mM $MgCl_2$, 1 mM $CaCl_2$, 0.1% microelement solution (from CM medium)). The mixture was incubated at RT for 1 to 30 min, then loading dye was added and samples were run on a 1-2 % agarose gel.

To test nuclease activity in the filtrate of an *S. indica* culture, a 5-day-old CM culture was minced and incubated for an additional 3 days. The culture was filtered through Miracloth (Millipore Merck, Darmstadt, Germany), and 50 μl of culture filtrate was added to linearized plasmid DNA, gDNA, or RNA.

### *Si*NucA-HA-His purification

A 7-day-old liquid culture of *S. indica* grown in CM medium was filtered through Miracloth. The mycelium was washed with 0.9% NaCl and minced in fresh CM medium in a mixer (MicrotronR MB550 homogenizer (Kinematica, Lucerne, Switzerland)). The culture was regenerated for two days. Subsequently, the culture was filtered with Miracloth and through a 0.45 μm membrane filter. To this cell-free culture filtrate, 1 mM phenylmethanesulfonylfluoride fluoride (PMSF) was added and the pH was adjusted to pH 7 with 1 M Tris pH 8. Proteins were precipitated with 80% ammonium sulfate. The protein pellet was resuspended in 20 mM Tris pH 8. Proteins were separated by size exclusion chromatography (Sephadex G 200 column, Hiload 6/600) using a 20 mM Tris pH 8 / 150 mM NaCl buffer. Fractions containing *Si*NucA-HA-His were desalted by dialysis and checked by SDS-PAGE and anti-HA Western blot. The protein was stored in 20 mM Tris pH 8. The identity of the protein was verified by LC-MS/MS.

### Measurement of enzyme kinetics of *Si*E5NT

*Si*E5NT fused to a C-terminal hemagglutinin (HA) and Strep tag (pXCScpmv-HAStrep, V69) was transiently expressed in *Nicotiana benthamiana* and purified by affinity chromatography as described by Werner et al.[63] and Myrach et al.[64] Enzyme concentrations were determined using bovine serum albumin standards after SDS-PAGE and Coomassie Blue staining with an Odyssey Fc Dual Mode Imaging System (Li-cor Biosciences, Germany).

To determine substrate specificity, different substrates were tested. Briefly, 10 μl of purified enzyme (1.9 x $10^{-4}$ mg protein) was added to 70 μl of reaction buffer (10 mM MES buffer, pH 6.0; 1 mM $CaCl_2$ and 1 mM $MgCl_2$) and pre-incubated for 5 minutes. Substrates were added (20 μl of a 5 mM stock solution) to give a final reaction volume of 100 μl. The reaction was quenched with 400 μl of MeOH at the indicated times and centrifuged for 10 min at 21,000g at 4°C. The supernatant was evaporated in a vacuum concentrator and the dry pellet resuspended in 100 μl of HPLC mobile phase A.

Samples were analyzed using an Agilent 1200 SL HPLC system equipped with a diode array detector. 10 μl of the sample was injected onto a Supelcosil LC-18-T column (Sigma-Aldrich) at a flow rate of 0.8 ml $min^{-1}$ and a column temperature of 25°C. The analytes were separated with the following gradient: 0 min, 100% A; 9 min, 100% A; 15 min, 75% A; 17.5 min, 10% A; 19 min, 0% A; 23 min, 0% A; 24 min, 100% A; 30 min, 100% A. Mobile phase A consisted of 100 mM $KH_2PO_4$, pH 6.0, in deionized water and mobile

phase B consisted of 90% 100 mM $KH_2PO_4$, pH 6.0, in deionized water and 10% MeOH. Appropriate standard solutions were used for quantification. Data were analyzed using Agilent Chemstation software.

Kinetic constants for deoxyadenosine monophosphate and adenosine monophosphate were determined using the EnzCheck (Thermo Fisher Scientific, Waltham, USA) phosphatase assay kit according to specifications, using only one-tenth of the recommended reaction volume.

### Measurement of release of deoxynucleosides

10 μg of salmon sperm DNA was incubated with 4 μl of *Si*NucA, 10 μl of *Si*E5NT, or a combination of both in a final volume of 40 μl containing 10 mM HEPES, pH 7.2; 100 mM $MgCl_2$; and 1 mM DTT. The enzymes were incubated in the buffer mixture for 5 minutes prior to the addition of DNA. The reaction was incubated at 22 °C for 1 hour and inactivated at 95 °C for 5 minutes. Subsequently, centrifugation was performed at 40000 g and 4 °C for 20 minutes. 20 μl of the supernatant was analyzed on a 2% agarose gel. The remaining 20 μl of the supernatant was mixed with 50 μl of water and used for HPLC MS/MS analysis. Samples and standards were analyzed using an Agilent 1290 Infinity II HPLC system coupled to an Agilent 6470 triple quadrupole mass spectrometer. Analytes (10 μl samples) were separated on a 50 x 4.6 mm Polaris C18A column (Agilent) using the following gradient: 0 min, 96% A; 8 min, 35% A; 8.2 min, 0% A; 10 min, 0% A; 10.1 min, 96% A. Mobile phase A consisted of 10 mM ammonium acetate, pH 7.5, and mobile phase B was pure MeOH. The flow rate was 0.6 ml $min^{-1}$ and the column temperature was 30°C. In-source parameters were set as previously described for deoxynucleoside analysis.[65] All analytes were measured in positive mode. Transitions (precursor and production), collision energies, and fragmentor energies are listed in Table S9.

### PAM fluorometric measurements

PAM fluorometry measurements were performed by transferring 9-day-old Arabidopsis seedlings into 24 well plates containing 2 ml of 2.5 mM MES buffer (pH 5.6). 3 seedlings were pooled in one well. After 24 hours of regeneration, seedlings were treated with solutions of 5' deoxyadenosine (dAdo), adenosine (Ado), or methyl jasmonate (all Sigma-Aldrich, Taufkirchen, Germany), adjusting to a final concentration of 500 μM. Treated seedlings were incubated in complete darkness for 20 min to reach a dark-adapted condition. The photosynthetic activity of the plants was measured using the M-Series PAM fluorometer (Heinz Walz GmbH, Effeltrich, Germany). Data were analyzed using ImagingWin software (v.2.41a; Walz, Germany). When further analysis of photosynthetic area development was required, it was evaluated using Fiji (ImageJ).[56]

### Cell death staining with Evans blue

A modified protocol as described in Vijayaraghavareddy et al.[66] was used. To quantify cell death induced by *S. indica* in *Arabidopsis*, plants were used for cell death staining at three time points, 7, 10, and 14 days after fungal spore inoculation, using five plants per treatment. For cell death induced by dAdo (or chemically induced cell death), plants were microscoped after 4 days of cell death treatment. To remove external fungal growth or chemical treatment solutions, plants were washed three times in $ddH_2O$ before cell death staining in a 2.5 mM Evans blue solution (Sigma-Aldrich, lot #MKCH7958) dissolved in 0.1 M $CaCl_2$ pH 5.6 for 15 minutes. After extensive washing for one hour with $ddH_2O$, images were captured using a Leica M165 FC microscope.

### Activity-based protein profiling

After treatment with 500 μM dAdo, 500 μM Ado, or MES buffer, 9-day-old Arabidopsis seedlings were frozen in liquid nitrogen, ground, and dissolved in 50 mM Tris-HCl buffer (pH 7). After centrifugation, the supernatant was divided and treated with either the proteasome inhibitor MG132 (final concentration: 50 μM, company) or DMSO for 30 min. Samples were then incubated with 26S proteasome probe MVB072 (final concentration: 1 μM, company): 1 μM,[27] Samples were then denatured in SDS loading dye at 95 °C and separated on 12% SDS gels. The probe was visualized using the rhodamine settings (excitation: 532 nm, emission: 580 nm) on a ChemiDoc (BioRad, CA, USA). The protein content of the samples was visualized by staining the gel with SYPRO™ Ruby (Invitrogen, Carlsbad, CA, USA) according to the manufacturer's instructions.

### RNAseq

7-day-old seedlings were transferred from plates to individual wells of 24-well plates containing 0.5 ml of liquid ½ MS medium containing 0.5% (w/v) sucrose. After 5 additional days in liquid culture, the medium was replaced with 1 ml of 500μ M dAdo in 2.5 mM MES buffer pH 5.6 or 2.5 mM MES buffer pH 5.6 alone as a negative control. Three replicates of four seedlings were harvested for each treatment at 0, 3, and 12 h after treatment (hpt), frozen in liquid nitrogen, and stored at -80° C until processing for RNA extraction. Total RNA was extracted using TRIZOL reagent as described above. RNA integrity was confirmed by gel electrophoresis, and quantity and purity were determined using a NanoDrop 2000. Stranded mRNA-seq libraries were prepared according to the manufacturer's instructions (Vazyme Biotech Co., Nanjing, China). Qualified libraries were sequenced on a HiSeq 3000 system instrument in the Genomics and Transcriptomics Laboratory at Heinrich Heine University to generate >100 million reads with a read length of 150 bp from three biological replicates. Trimmomatic v. 0.36,[57] was used for quality trimming and adapter clipping. Reads were then mapped to Arabidopsis TAIR10 CDS assembly and quantified using kallisto v. 0.46.2,[58] resulting in estimated counts and transcripts per million (TPM) values. The $\log_2$ fold difference in gene expression between conditions was estimated using the R packages tximport[59] and DESeq2.[60] Genes with statistical significance were selected (FDR-adjusted p-value < 0.05). Data have been deposited at NCBI under GEO accession number GSE209761 and GSM6394981.

### Collection of extracellular fluid

7-day-old Arabidopsis seedlings germinated on ½ MS agar containing 1% sucrose were transferred to 24 well plates. Each well contained 3 seedlings in 1.5 ml of 2.5 mM MES and the specific treatment. After transfer, the plants were returned to the growth chamber for three days. The seedlings were then removed and the liquid centrifuged at 4000 g for 15 minutes. The supernatant was freeze dried and sent for metabolite analysis.

### Metabolite analysis

5 μl of the apoplastic liquid was injected into an Acquity UPLC (Waters Inc.) equipped with a Nucleoshell RP18 column (Macherey and Nagel, 150mm x 2 mm x 2.1μm) using tributylammonium as the ion pairing agent. Solvent A: 10 mM tributylamine (aqueous) acidified with glacial acetic acid to pH 6.2; solvent B acetonitrile. Gradient: 0-2 min: 2% B, 2-18 min 2-36% B, 18-21 min 36-95% B, 21-22.5 min 95% B, 22.51-24 min 2% B. Column flow was 0.4 ml $min^{-1}$ throughout. The column temperature was 40 °C. Scheduled metabolite detection based on multiple reaction monitoring (MRM) was performed in negative mode with electrospray ionization (ESI) on a QTrap 6500 (AB-Sciex GmbH, Darmstadt, Germany): Ion source gas 1: 60 psi, ion source gas 2: 70 psi, curtain gas: 35 psi, temperature: 450 °C, ion spray voltage floating: and -4500V). MRM transitions of 189 metabolites covering central carbon and energy metabolism were previously signal optimized and retention times determined (Table S10).

### $Ca^{2+}$ influx quantification

Calcium influx assays were performed as previously described in Wanke et al.[67] Briefly, individual 7-day-old Arabidopsis seedlings were placed in white 96-well plates filled with 200 μl reconstitution buffer (2.5 mM MES pH 5.7 [Sigma-Aldrich, Taufkirchen, Germany], 10 mM $CaCl_2$ [Roth, Karlsruhe, Germany]). Before incubation overnight in the dark, the solution was replaced with 133 μl reconstitution buffer containing 10 mM coelenterazine (Roth, Karlsruhe, Germany). The following day, chemiluminescence was measured using a TECAN SPARK 10M microplate reader. After baseline measurement, 67 μl of three-fold concentrated elicitor solutions (or Milli-Q water as a sham control) were added manually. Cytosolic calcium influx after addition of the trigger was measured continuously for 30 min. To determine the undischarged aequorin for treatment normalization, 100 μl 3 M $CaCl_2$ (in 30% EtOH) was injected into each well, followed by constant measurement for 1 minute. All steps were performed with an integration time of 450 msec.

### Heterologous protein production in *Nicotiana benthamiana* and protein purification

For heterologous protein production in Nicotiana *benthamiana*, leaves of 4-week-old plants *were* infiltrated with *Agrobacterium tumefaciens* GV3101 strains. *A. tumefaciens* was grown in LB liquid medium with the appropriate antibiotics at 28°C and 180 rpm for 2 days until an $OD_{600}$ of 1 was achieved. Cultures were centrifuged at 3500 rpm for 15 min at RT, the supernatant was discarded and resuspended in 1 ml infiltration buffer (10 mM MES pH 5.5, 10 mM $MgCl_2$, 200 μM acetosyringone) and incubated for 1 h in the dark at 28°C, 180 rpm. All strains were diluted with the infiltration buffer to an $OD_{600}$ of 1. Each strain was mixed with P19-expressing strains at a 1:1 ratio. 2-3 leaves per plant were infiltrated with a needleless syringe. After 4 dpi, leaves were separated from the plant and crushed in liquid nitrogen. Protein purification was performed according to Werner et al.[63] with minor modifications performed: A 15-ml tube was filled to the 2-ml mark with ground leaf material, and 2 ml of cold extraction buffer (100 mM Tris pH 8.0, 100 mM NaCl, 5 mM EDTA, 0.5% Triton X100, 10 mM DTT, 100 μg/ml avidin) was added. The powder was resuspended by vortexing and then centrifuged at 12000 rpm and 4°C for 10 minutes. The supernatant was transferred to a new tube and 100 μl of Strep-Tactin® Macroprep (50% slurry) was added and incubated for 60 min at 4°C in a rotating wheel. The mixture was centrifuged at 700xg at RT for 30 s and the supernatant was completely removed from the beads. The beads were washed once with 4 ml and two additional times with 2 ml of wash buffer (50 mM Tris pH 8.0, 100 mM NaCl, 0.5 mM EDTA, 0.005% Triton X-100, 2 mM DTT) by centrifugation for 30 s at 700xg and the supernatant was discarded. During the final wash, beads were transferred to a 1.5 ml tube with a low binding level. The beads were either boiled directly for 5 min at 95°C with 6x SDS loading dye to run on an SDS-PAGE, or the proteins were eluted from the beads by adding 100 μl of elution buffer (wash buffer + 2.5 - 10 mM biotin) and incubating at 25°C, >800 rpm for 5 min. Samples were centrifuged at 700xg for 20 s and elution was repeated. Elution fractions were pooled, SDS loading dye was added, and samples were run on SDS-PAGE followed by Western blot.

### Ion leakage measurements

The seedlings for measurement of ion leakage were prepared in the same manner as seedlings for PAM fluorometry measurements. Ion leakage was measured with a conductivity meter (LAQUAtwin EC-11; Horiba, Newhampton, UK).

### Seed germination test

Sterile Arabidopsis seedlings were transferred into 24-well plates containing 2 ml of 1/10 PNM medium. The medium contained either 500 μM dAdo or the same volume of 2.5 mM MES (pH 5.6). Ten seeds were placed in each well and grown under short-day conditions after 2 days of stratification. Seedling growth was monitored by PAM fluorometry.

### Root length measurements

To evaluate root length, scans of the square plates containing seedlings were analyzed using Fiji (ImageJ) and the length of the primary root was measured.

### Oxidative burst assay

Individual 7-day-old Arabidopsis seedlings were transferred to white 96-well plates containing 200 μl reconstitution buffer (2.5 mM MES pH 5.7 (Sigma-Aldrich, Taufkirchen, Germany), 10 mM $CaCl_2$ (Roth, Karlsruhe, Germany) and incubated overnight in the growth chamber. The following day, the buffer was replaced with 133 μl reconstitution solution containing 15 $\mu g ml^{-1}$ horseradish peroxidase (Sigma-Aldrich, Taufkirchen, Germany) and 15 μM L-O12 (Wako Chemicals, Neuss, Germany). After 10 min incubation, 67 μL of three-fold concentrated elicitor solutions (or Milli-Q water as a mock control) were added manually to the wells. Measurements were started immediately and chemiluminescence was measured continuously with a TECAN SPARK 10M microplate reader (Tecan, Männedorf, Switzerland) at an integration time of 450 ms.

### Protoplast isolation and transformation

As described in Ochoa-Fernandez et al.,[68] protoplasts were isolated from 2-week-old *A. thaliana* seedlings (Col-0, *isi, ent3*) grown in 12 cm square plates containing SCA medium (0.32 % (wt/vol) Gamborg's B5 basal salt powder with vitamins (bioWORLD), 4 mM $MgSO_4x7H_2O$, 43.8 mM sucrose and 0.8% (wt/vol) phytoagar in $H_2O$, pH 5.8, autoclaved, 0.1% (vol/vol) Gamborg's B5 Vitamin Mix (bioWORLD), with a 22 °C, 16-h light – 8-h dark cycle. The leaf material was sliced with a scalpel and incubated in darkness at 22 °C overnight in MMC solution (10 mM MES, 40 mM $CaCl_2H_2O$, 467 mM mannitol, pH 5.8, sterile filtered) containing 0.5% cellulase Ono- zuka R10 and macerozyme R10 (SERVA Electrophoresis). After 18h, the lysate was thoroughly mixed, passed through a 70 mm pore size sieve and transferred to a MSC solution (10 mM MES, 0.4 M sucrose, 20 mM $MgCl_2$ $6H_2O$, 467 mM mannitol, pH 5.8, sterile filtered) and carefully overlaid with MMM solution (15 mM $MgCl_2$, 2.5 mM MES, 467 mM mannitol, pH 5.8, sterile filtered). After centrifugation the protoplasts were collected at the interphase and transferred to a W5 solution (2 mM MES, 154 mM NaCl, 125 mM $CaCl_2x2H_2O$, 5 mM KCl, 5 mM glucose, pH 5.8, sterile filtered) and diluted to $10^6$ protoplasts per 100 ml after counting in a Rosenthal chamber. The plasmids were transferred by PEG-mediated transformation. 10 μg of plasmid DNA (pSW209 – firefly luciferase reporter; pGEN016 - Stuffer; pGWB502 N-TIR; pGWB502N-trunc TIR) were used to transform 1,000,000 protoplasts in non-treated 6-well plates by drop-wise addition of a PEG solution (4 g $PEG_{4000}$, 2.5 ml of 800 mM mannitol, 1 ml of 1 M $CaCl_2$ and 3 ml $H_2O$). After 8-min incubation, 120 ml MMM and 1,8 ml PCA (0.32% (wt/vol) Gamborg's B5 basal salt powder with vitamins (bioWorld), 2 mM $MgSO_4x7H_2O$, 3.4 mM $CaCl_2x2H_2O$, 5 mM MES, 0.342 mM l-glutamine, 58.4 mM sucrose, 444 mM glucose, 8.4 mM calcium pantothenate, 2% (vol/vol) biotin from a biotin solution 0.02% (wt/vol) 0.1% (vol/vol) in $H_2O$, pH 5.8, sterile filtered, 0.1% (vol/ vol) Gamborg's B5 Vitamin Mix, 64.52 mg $ml^1$ ampicillin), were added to a final volume of 2 ml protoplast suspension. 3 hours after transformation 0.9 ml of protoplast were transferred to non-treated 12 well plates and induced with dAdo (0μM, 25μM, 50μM, 100μM). The protoplasts were kept in darkness for 18 h at 22°C.

Four technical replicates of 80 ml protoplast suspensions were pipetted into a 96-well white flat-bottom plates (Costar) for determination of activity luciferases as indicator for cell death. Addition of 20 ml of FLuc substrate (0.47 mM d-luciferin (Biosynth AG), 20 mM tricine, 2.67 mM $MgSO_{4x}7H_2O$, 0.1 mM EDTA $2H_2O$, 33.3 mM dithiothreitol, 0.52 mM adenosine 5'-triphosphate, 0.27 mM acetyl–coenzyme A, 5 mM NaOH, 264 mM $MgCO_3x5H_2O$, in $H_2O$, pH 8) was performed prior to luminescence determination in a plate reader (determination of 20-min kinetics, integration time 0.1 s).

## QUANTIFICATION AND STATISTICAL ANALYSIS

To evaluate significant differences, ANOVA with post-hoc Tukey HSD test or Student's t-test were used in this study. Statistical analyses were performed using GraphPad Prism. Statistical details of the experiments can be found in the figure legends.